Powder neutron diffraction study of phase transitions in and a phase diagram of $(1-x)[Pb(Mg_{1/3}Nb_{2/3})O_3]$-$xPbTiO_3$

Akhilesh Kumar Singh and Dhananjai Pandey*
School of Materials Science & Technology, Institute of Technology, Banaras Hindu University, Varanasi-221 005, India

Oksana Zaharko
Laboratory for Neutron Scattering, Paul Scherrer Institute, CH-5232 Villigen PSI, Switzerland
(Received 27 June 2005; revised manuscript received 6 May 2006; published 7 July 2006)

Dielectric, piezoelectric resonance frequency, and powder neutron diffraction studies as a function of temperature have been performed on several compositions of $(1-x)[Pb(Mg_{1/3}Nb_{2/3})O_3]$-$xPbTiO_3$ (PMN-xPT) ceramics in and outside the morphotropic phase boundary (MPB) region to investigate the phase transitions and phase stabilities in this mixed system. Anomalies in the temperature dependence of piezoelectric resonance frequency and dielectric constant are correlated with structural changes using Rietveld analysis of powder neutron diffraction data. The frequency dependent dielectric studies reveal relaxor ferroelectric behavior for $x<0.35$ and a normal ferroelectric behavior for $x\geqslant 0.35$. The dielectric peak temperature and the Vogel-Fulcher freezing temperature are found to increase linearly with "x" while their difference, after decreasing linearly with x, vanishes at $x=0.35$ suggesting a crossover form relaxor ferroelectric to normal ferroelectric behavior at this composition. A phase diagram of the PMN-xPT system showing the stability fields of ergodic relaxor, monoclinic M_B, monoclinic M_C, tetragonal and cubic phases is presented. Our results suggest the presence of a succession of three phase transitions, not reported earlier, corresponding to structural changes from the monoclinic M_B to the monoclinic M_C to the tetragonal to the cubic phases for $0.27\leqslant x\leqslant 0.30$ on heating above room temperature. In addition, our studies confirm the earlier findings on transitions from the monoclinic M_C to the tetragonal to the cubic phases for $0.31\leqslant x\leqslant 0.34$ on heating above room temperature and tetragonal to monoclinic M_C phase on cooling below room temperature for $x=0.36$. All these transitions are found to be accompanied with anomalies either in the temperature dependence of dielectric constant or the piezoelectric resonance frequency or both. Rietveld analyses of the powder neutron diffraction data at *various* temperatures on a pseudorhombohedral composition with $x=0.25$ suggest that the short range M_B type monoclinic order present at room temperature grows to long range monoclinic order on lowering the temperature. The temperature variations of the unit cell parameters and atomic shifts are also presented to throw light on the nature of the various phase transitions in this mixed system.

DOI: 10.1103/PhysRevB.74.024101 PACS number(s): 77.84.Lf, 82.35.Jk, 77.84.Dy, 61.12.−q

I. INTRODUCTION

Solid solution systems like $Pb(Zr_xTi_{1-x})O_3$ (PZT), $(1-x)Pb(Mg_{1/3}Nb_{2/3})$-$xPbTiO_3$ (PMN-xPT) and $(1-x)Pb(Zn_{1/3}Nb_{2/3})$-$xPbTiO_3$ (PZN-xPT) etc. are technologically important for piezoelectric transducer and actuator applications.[1] The phase diagram of these mixed systems exhibits a morphotropic phase boundary (MPB) which has until recently been believed to separate the rhombohedral (R) and tetragonal (T) phase fields.[2] The MPB is of special significance for technological applications since the electromechanical response of these materials is found to be maximum for the MPB compositions.[2] Until recently, it has been believed that the rhombohedral and tetragonal phases with $R3m$ and $P4mm$ space groups, respectively, coexist in the MPB region.[2–6] In recent years, several monoclinic phases have been discovered[7–13] in these MPB ceramics, some of which have been confirmed to be present in the MPB region itself.[7,8,10,11] The discovery of the monoclinic phases in the MPB systems has catalyzed several exciting experimental[14–20] and theoretical developments.[21,22] Interesting field induced phase transitions were discovered in PZT,[14] PMN-xPT,[15,16] and PZN-xPT,[17] highlighting the important role of the intermediate monoclinic phase for the large electromechanical response of these materials. Optical studies have revealed domain patterns characteristic of the monoclinic phases in these mixed systems.[18–20] Theoretical first principles calculations and phenomenological theory considerations have not only confirmed the existence of monoclinic phases in the MPB region[21,22] but also revealed the dominant role of rotational instabilities of polarization vector across the MPB compositions.[21] Further, phenomenological theory considerations have shown that the Devonshire free energy expansion upto the eighth-order term is needed to stabilize the monoclinic phases indicating the highly anharmonic nature of these materials.[22] All these studies have also led to significant modifications of the phase diagrams of these solid solution systems.[23–25]

Among the three strongly piezoelectric MPB systems viz PZT, PZN-xPT, and PMN-xPT, the PMN-xPT is the most attractive because it can be easily prepared both in single crystal as well as ceramic forms whereas it is difficult to prepare PZT single crystals and PZN-xPT ceramics. In the PMN-xPT system, Singh and Pandey[10] first reported an M_C type monoclinic phase (in the notation of Vanderbilt and Cohen[22]) with Pm space group in the MPB region at $x=0.34$. Soon afterwards, they[11] presented evidence for the presence of another monoclinic phase with space group Cm

in the MPB region in between the rhombohedral and monoclinic *Pm* phase fields. It was shown[11] that the monoclinic *Cm* phase of PMN-*x*PT is of M_B type in the notation of Vanderbilt and Cohen[22] in contrast to the M_A type with identical space group previously reported in the $Pb(Zr_xTi_{1-x})O_3$ (PZT) ceramics.[7,8] The components of the polarization vectors, $\mathbf{P_x}$, $\mathbf{P_y}$, $\mathbf{P_z}$, along the three pseudocubic axes bear different relationships for the M_A and M_B phases, viz. $\mathbf{P_x}=\mathbf{P_y}<\mathbf{P_z}$ for M_A and $\mathbf{P_x}=\mathbf{P_y}>\mathbf{P_z}$ for M_B.[22] Temperature and electric field dependent optical domain structure studies on PMN-*x*PT single crystals by Tu *et al.*[27,28] also suggest the presence of a monoclinic *Cm* phase. Using Rietveld analysis of x-ray powder diffraction data, the compositional range of the stability of the different crystallographic phases of the PMN-*x*PT at room temperature has been precisely located by Singh and Pandey.[11] It has been shown[11] that the structure of the PMN-*x*PT is rhombohedral (*R*) for $x<0.27$, monoclinic with space group *Cm* (M_B type) for $0.27\leqslant x\leqslant 0.30$, monoclinic with space group *Pm* (M_C type) for $0.30<x<0.35$ and tetragonal (*T*) for $x\geqslant 35$. The presence of the monoclinic M_C phase in the MPB region of the PMN-*x*PT has since been confirmed using synchrotron x-ray diffraction (XRD) studies also Ref. 24. Further, a high-resolution powder neutron diffraction study by Singh *et al.*[26] has unambiguously confirmed the stability of the second monoclinic phase of M_B type. Thus, the sequence of structural phases appearing at room temperature with increasing Ti^{4+} content in the PMN-*x*PT system is R-M_B-M_C-T. Theoretical phase diagram of Vanderbilt and Cohen[22] supports the possibility of such a sequence of phase transition as a function of composition from the point of view of continuous rotation of the polarization vector between [001] and ⟨111⟩ pseudocubic directions of the tetragonal and rhombohedral phases. Evidence for an M_B phase has also been obtained by Viehland and Li[29] in their field induced transition studies on a PMN-0.30PT crystal. Using experimental data of Singh and Pandey[11] and Noheda *et al.*,[24] Topolov and Ye[30] have verified the important role of these intermediate M_B and M_C monoclinic phases and the phases coexisting with them across the MPB in relieving the mechanical stresses and providing the elastic matching of the strains at the various interphase boundaries.

In addition to the stability of the M_C phase at room temperature in the composition range $0.31\leqslant x\leqslant 0.34$,[10,11] this phase has been reported at low temperatures also as a result of a phase transition from the room temperature tetragonal phase for $x\geqslant 0.35$, as shown by Kiat *et al.*[12] for $x=0.35$ and Noheda *et al.* for $x=0.35$ and 0.37.[24] Kiat *et al.*[12] confirmed the M_C phase at low temperatures using Rietveld analysis of powder neutron diffraction data for $x=0.35$. Noheda *et al.*[24] did not use Rietveld technique and their conclusion about the M_C phase is based on the profile analysis of the synchrotron data of a few selected reflections. No attempt was made by Noheda *et al.*[24] or Kiat *et al.*[12] to study the temperature dependence of the atomic displacements which constitute the microscopic order parameter. Based on the temperature variation of the cell parameters, Noheda *et al.*[24] have reported a new phase diagram of PMN-*x*PT which includes the stability region for the monoclinic M_C phase, earlier discovered by Singh and Pandey,[10] along with those for the rhombohedral and tetragonal phases. However, this tentative phase diagram of PMN-*x*PT (Ref. 24) needs to be modified in view of the subsequent discovery of the monoclinic M_B phase by Singh and Pandey[11] and Singh *et al.*[26] Another limitation of the phase diagram proposed by Noheda *et al.*[24] is that the phase boundaries were determined on the basis of the temperature variations of unit cell parameters only which cannot be reliable on account of the large coexistence regions accompanying these transitions.[11,24] The present work contains the results of a comprehensive study on PMN-*x*PT ceramics with the objective of not only settling the phase diagram aspects but also several other outstanding issues outlined below.

Singh and Pandey[11] observed two peaks in the composition dependence of room temperature dielectric constant (ε') around $x\approx 0.30$ and $x\approx 0.35$ corresponding to the *Cm-Pm* (M_B-M_C) and *Pm-P*4*mm* (M_C-T) phase boundaries. Similarly, Guo *et al.*[31] found evidence for two peaks in d_{33} versus x plot for single crystals of PMN-*x*PT at compositions exactly matching with the earlier observation of two peaks by Singh and Pandey[11] for the ε' versus x plot. There is no satisfactory explanation as to why the plot of dielectric constant and d_{33} coefficient against composition (x) at room temperature shows two peaks[11,31] corresponding to the *Cm-Pm* and *Pm-P*4*mm* phase boundaries at $x\approx 0.30$ and $x\approx 0.35$, respectively, but none corresponding to the *R*3*m* -*Cm* phase boundary at $x\approx 0.27$. We attribute this to the presence of short range M_B type monoclinic order in the so-called rhombohedral compositions at room temperature. These short-range ordered monoclinic regions are found to grow on lowering the temperature, as revealed by profile analysis of the diffraction data at various temperatures.

The temperature dependent dielectric studies on PMN -*x*PT by earlier workers[3,4,32–34] have revealed two dielectric anomalies in poled ceramics and single crystals for PMN rich compositions near the MPB. One of these anomalies is strong and corresponds to the main Curie peak whereas the second one is rather weak. There is considerable controversy about the origin of the weak anomaly in ε'(T) and several different explanations based on depoling,[32] Vogel-Fulcher freezing,[33] and rhombohedral to tetragonal phase transition[3,34] have been advanced in the literature. We report here the observation of a weak dielectric anomaly even in unpoled PMN-*x*PT ceramics which cannot be attributed to any one of the three reasons proposed by the earlier workers. Experimental evidences are presented to demonstrate that this anomaly is linked with a monoclinic M_C to tetragonal phase transition.

To settle the issues outlined above, we present here the results of temperature dependent dielectric constant and piezoelectric resonance frequency to study the phase transition behavior of several PMN-*x*PT compositions across the MPB. We then correlate the temperatures corresponding to the anomalies in the dielectric constant and/or piezoelectric resonance frequency with structural changes using Rietveld analysis of temperature dependent powder neutron diffraction data. Powder neutron diffraction data is needed since the x-ray diffraction data cannot help determine the sense of relative displacements of titanium and oxygen atoms uniquely, as was first noted by Shirane *et al.*[35] in the context of the structure determination of the tetragonal phase of pure

$PbTiO_3$. To the best of our knowledge, there is no report dealing with the temperature dependence of the atomic displacements in various crystallographic phases of PMN-*x*PT. In the present work, we have investigated this aspect also and have studied the microscopic order parameter (i.e., the displacements of cations and anions with respect to their symmetric positions) as calculated from the coordinates obtained by Rietveld refinements at various temperatures. We use our results to modify the existing phase diagram of PMN-*x*PT (Ref. 24) by incorporating the phase fields of the monoclinic *Cm* and *Pm* phases.

II. EXPERIMENTAL

A. Sample preparation

Chemically homogeneous and stoichiometric samples containing only the perovskite phase of PMN-*x*PT were prepared by a newly developed method[36] without using any excess amount of MgO or PbO, in contrast to the generally followed methods where one uses excess amount of PbO and MgO to avoid the formation of the unwanted pyrochlore phase.[5,24,37] The Columbite precursor $MgNb_2O_6$ was prepared by calcining a stoichiometric mixture of $MgCO_3.3H_2O$ and Nb_2O_5 at 1050 °C for 6 h. Stoichiometric amount of TiO_2 was mixed in the next step with $MgNb_2O_6$ and calcined at 1050 °C for 6 h to obtain $(1-x)/3MgNb_2O_6$-$xTiO_2$ (MNT) precursors. This MNT precursor was then mixed with the stoichiometric amount of $PbCO_3$, and calcined at 750 °C for 6 h, to obtain PMN -*x*PT powders. The as-calcined powders were compacted into the form of circular pellets of 12 mm diameter and 1.5 mm thickness at an optimum load of 65 kN. Sintering was carried out at 1150 °C for 6 h in PbO atmosphere. The weight loss due to possible PbO evaporation was less than 0.2% and the sintered densities were close to 99% of the theoretical density. Sintered pellets were crushed into fine powders and annealed at 500 °C for 10 h to remove the strains introduced during crushing. The annealed powders were used in the neutron diffraction measurements.

B. Dielectric and piezoelectric resonance frequency measurements

For dielectric measurements top and bottom surfaces of the sintered pellets were polished gently with 0.25 μm diamond paste, cleaned with isopropyl alcohol and then electroded with fired-on silver paste which was first dried at 150 °C and then cured at 500 °C for 5 min. For piezoelectric measurements, the electroded pellets were poled at a field of 35 kV/*Cm* at 50 °C for 1 h and then cooled to room temperature with field applied. The piezoelectric resonance (f_r) and antiresonance (f_a) frequencies were measured in the planar mode by finding out the maximum and minimum value of impedance as a function of frequency using a Solartron Impedance Gain Phase Analyzer (Model 1260). The capacitance and tan δ values at various frequencies were measured using Hioki 3532 LCR-Hitester. The temperature of the sample in these measurements was controlled within ±1 °C using an Eurotherm (Model 2416) programmable temperature controller. Temperature of the sample was varied at a rate of 1.5 °C/min during the dielectric constant and piezoelectric resonance frequency measurements.

C. Neutron data collection

High-resolution neutron powder diffraction patterns were recorded on a HRPT diffractometer at **SINQ**, Switzerland with a wavelength of 1.154 Å. The diffractometer is equipped with 1600 detectors, covering a range of 160° scattering angle. For the used set up (collimations $\alpha_1=12'$, $\alpha_2=24'$), the best resolution of $\Delta d/d=0.0013$ is achieved for the scattering angle interval 120°–140°. The patterns below room temperature were recorded by cooling the sample in the closed cycle refrigerator. The high temperature patterns were recorded by heating the sample in the radiation furnace. The powders were packed into cylindrical shape Al containers with 8 mm diameter.

D. Rietveld refinement details

Rietveld refinement of the powder neutron diffraction data in the 2θ range 14 to 155° was carried out using DBWS-9411 and Fullprof programmes.[38] Pseudo-Voigt function was used to model the peak profiles. We have used isotropic peak shape function because there is a risk of structural features falsely being modeled in terms of anisotropic peak broadening while using anisotropic peak shape function. Background was estimated using linear interpolation method between fixed values. Except for the occupancy parameters of the atoms, which were fixed at the nominal composition, all other parameters, i.e., scale factor, zero correction, profile parameters, lattice parameters, and positional coordinates were refined. Anisotropic peak shape function was also considered for the *R*3*m* structure. The isotropic thermal parameter values for Pb were invariably found to be high. Use of anisotropic thermal parameters for Pb led to improvements in the agreement factors for monoclinic *Cm* phase. Other structures were refined using isotropic thermal parameter values. Use of anisotropic thermal parameters for Pb in the rhombohedral phase also led to improved *R* factors, however, *R* factors were inferior to those obtained for isotropic Pb-thermal parameters with local ⟨100⟩ displacements of Pb superimposed on [111] shift. In view of this, local displacements of Pb with isotropic thermal parameter were considered while refining rhombohedral structure.

In the cubic phase with the *Pm*3*m* space group, Pb occupies 1(a) sites at (0,0,0), Ti/Mg/Nb occupy 1(b) sites at $\left(\frac{1}{2},\frac{1}{2},\frac{1}{2}\right)$ and oxygen occupies 3(c) sites at $\left(\frac{1}{2},\frac{1}{2},0\right)$. In the tetragonal phase with *P*4*mm* space group, the asymmetric unit consists of four atoms with the Pb atom in 1(a) sites at (0,0, *z*), Ti/Nb/Mg and O_I in 1(b) sites at $(1/2,1/2,z)$, and O_{II} in 2(c) sites at $(1/2,0,z)$. The asymmetric unit of the monoclinic phase with space group *Pm* has got five atoms with Pb and O_I in 1(a) site at $(x,0,z)$, Ti/Nb/Mg, O_{II} and O_{III} in 1(b) sites at $(x,1/2,z)$. In the monoclinic phase with space group *Cm*, there are four atoms in the asymmetric unit with Pb, Ti/Nb/Mg, and O_I in 2(a) sites at $(x,0,z)$ and O_{II} in 4(b) sites at (x,y,z). For the rhombohedral phase with *R*3*m*

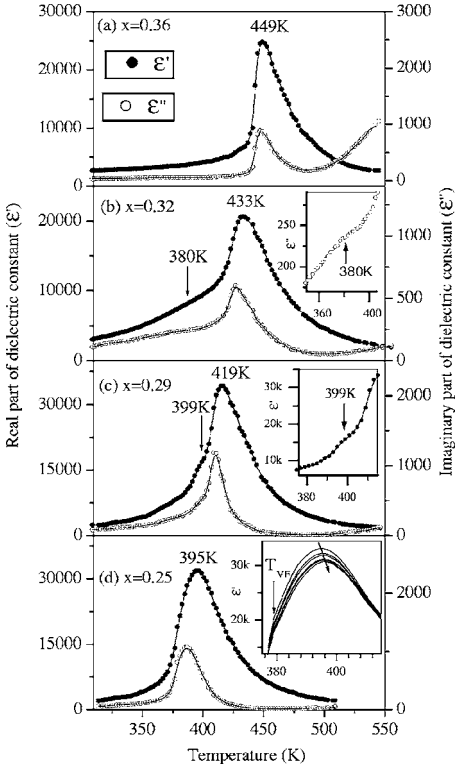

FIG. 1. Variation of the real (ε') and imaginary (ε'') parts of dielectric constant with temperature for upoled PMN-xPT ceramics measured at 1 kHz: (a) $x=0.36$, (b) $x=0.32$, (c) $x=0.29$, and (d) $x=0.25$. Insets in (b) and (c) illustrate weak dielectric anomaly corresponding to the monoclinic to tetragonal phase transition and inset in (d) shows shift in T_m' with increasing measuring frequency. The arrow at the main peak in this inset points to increasing frequencies of measurement (0.1, 0.5, 1, 5, 10, and 50 kHz). The second arrow shows the abrupt disappearance of the frequency dispersion at the Vogel-Fulcher freezing temperature (T_{VF}).

space group, we used hexagonal axes with lattice parameters $a_H=b_H=\sqrt{2}\,a_R$ and $c_H=\sqrt{3}\,a_R$ where a_R corresponds to the rhombohedral cell parameter. In the asymmetric unit of the rhombohedral phase Pb and Nb/Ti/Mg atoms occupy 3(a) sites at $(0,0,z)$ and O at the 9(b) site at $(x,2x,1/6)$. Pb was fixed at (0,0,0) for the cubic, tetragonal and monoclinic structures.

III. RESULTS AND DISCUSSION

A. Dielectric and piezoelectric resonance frequency (f_r) measurements

Phase transition studies on unpoled PMN-xPT ceramics were carried out above the room temperature using dielectric measurements for the composition range $0.25 \leqslant x \leqslant 0.39$ at $\Delta x=0.01$ interval. Fig. 1 depicts the temperature dependence of the dielectric constant of four PMN-xPT compositions with $x=0.25$, 0.29, 0.32, and 0.36, representative of the rhombohedral, monoclinic Cm, monoclinic Pm and tetragonal structures at room temperature, respectively. These measurements were carried out during heating above the room temperature. Filled and open circles in this figure correspond

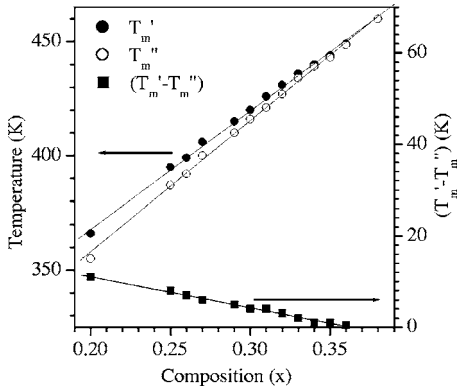

FIG. 2. Composition dependence of T_m', T_m'' and their difference ($\Delta T=T_m'-T_m''$) for PMN-xPT ceramics as obtained at 1 kHz.

to the real (ε') and imaginary (ε'') parts of the dielectric constant. It is evident from this figure that the dielectric anomaly for $x=0.36$ is relatively sharp while it is smeared out for the other three compositions. Furthermore, the temperatures T_m' and T_m'' corresponding to the peaks in the $\varepsilon'(T)$ and $\varepsilon''(T)$ plots are coincident (i.e., $T_m'=T_m''$) for $x=0.36$ whereas for the other compositions T_m'' is found to be less than T_m' ($T_m''<T_m'$). The fact that $T_m''<T_m'$ for $x \leqslant 0.32$ clearly points towards relaxor nature of the transition giving rise to the broad peak in $\varepsilon'(T)$.[39] For relaxor ferroelectrics, not only T_m'' is less than T_m' but both the peak temperatures also shift to higher side on increasing the measuring frequency due to relaxational freezing of the dipolar clusters.[39,40] This was indeed observed for the PMN-xPT compositions with $x<0.35$, and is illustrated in the inset for $x=0.25$ for $\varepsilon'(T)$. The composition dependence of T_m', T_m'' and their difference ($\Delta T=T_m'-T_m''$) as obtained at 1 kHz is shown in Fig. 2. It can be seen from this figure that the difference ΔT decreases with increasing PT content in PMN-xPT indicating a weakening of the relaxor features. With the addition of $PbTiO_3$ it is expected that the relaxor behavior will eventually give way to regular ferroelectric behavior since PMN is an archetypal relaxor ferroelectric whereas $PbTiO_3$ is a regular ferroelectric. It is also evident from Fig. 2 that $\Delta T=T_m'-T_m''$ vanishes around $x=0.35$ suggesting a crossover from relaxor ferroelectric to regular ferroelectric behavior at $x \approx 0.35$, in agreement with the results shown in Fig. 1 for $x=0.36$ where T_m' and T_m'' are coincident.

As said earlier in Sec. I, a weak dielectric anomaly below the main Curie peak has been reported by several workers in poled PMN-xPT ceramics and single crystals during heating.[3,4,32–34] This has been variously attributed to depoling,[32] Vogel-Fulcher freezing,[33] and rhombohedral to tetragonal structural phase transition.[3,4,34] We have also observed a weak dielectric anomaly preceding the main Curie peak in the composition range $0.27 \leqslant x \leqslant 0.34$ as depicted in the insets to Figs. 1(b) and 1(c) for $x=0.32$ and 0.29. This anomaly cannot be attributed to depoling process since the data presented in Fig. 1 correspond to measurements on unpoled ceramics. In order to decide whether this dielectric anomaly is due to Vogel-Fulcher freezing of polar clusters, we analyzed the frequency dispersion of imaginary part of

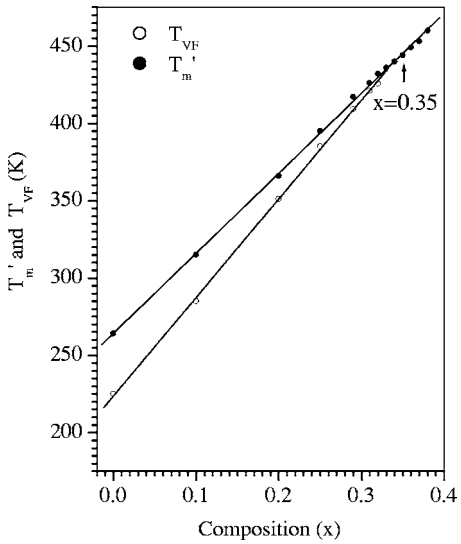

FIG. 3. Composition dependence of the Vogel-Fulcher freezing temperature (T_{VF}) and T_m' for PMN-xPT ceramics as obtained from the frequency dispersion of T_m''. Data points for pure PMN and PMN-0.10PT were adapted from Refs. 41 and 42.

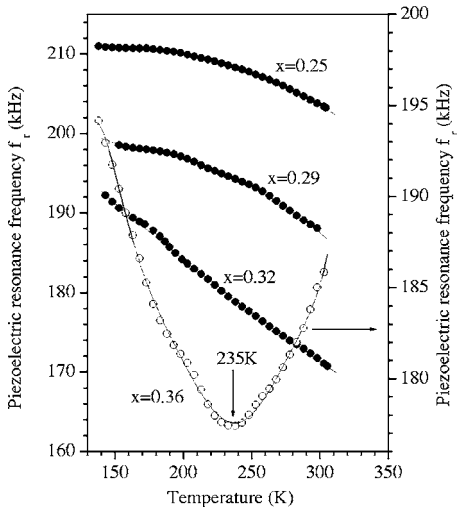

FIG. 4. Variation of piezoelectric resonance frequency (f_r) with temperature below 300 K for PMN-xPT ceramics with x=0.25, 0.29, 0.32, and 0.36. The anomaly around 235 K for x=0.36 corresponds to room temperature tetragonal to low temperature monoclinic M_C phase transition.

the dielectric constant which gave 426.7 K and 411.2 K as the Vogel-Fulcher freezing temperatures for x=0.32 and x=0.29. Both these temperatures are substantially higher than the temperatures 380 K and 399 K corresponding to the weak dielectric anomaly for x=0.32 and 0.29, respectively. Hence the week dielectric anomalies preceding the main Curie peak in Fig. 1 for x=0.32 and 0.29 cannot be attributed to Vogel-Fulcher freezing of the polar clusters. This leaves behind a structural phase transition as the only reason for this weak anomaly preceding the main Curie peak. As will be shown in the subsequent sections, this anomaly is linked with the monoclinic (M_B/M_C) to tetragonal phase transition and not with the rhombohedral to tetragonal phase transition assumed by earlier workers.[3,4,34]

Composition dependence of the Vogel-Fulcher freezing temperature, as obtained from the frequency dispersion of T_m'', is shown in Fig. 3 which also includes the freezing temperatures for pure PMN and PMN-0.10PT adapted from Refs. 41 and 42. It is interesting to note that the variation of Vogel-Fulcher freezing temperature with composition follows a linear relationship. Further, for $x \approx 0.35$, not only T_m' becomes equal to T_m'' (see Fig. 2) but also the T_{VF} versus x line on extrapolation meets the T_m' versus x line suggesting regular ferroelectric behavior for $x \geqslant 0.35$, in agreement with the results of Fig. 2.

Since all the compositions studied in the present work are ferroelectric at room temperature, it is expected that any phase transition occurring below room temperature will be from one ferroelectric phase to another ferroelectric phase. The low temperature transitions involving two ferroelectric phases do not give rise to prominent anomalies in $\varepsilon'(T)$ and $\varepsilon''(T)$.[43] It has been shown for PZT ceramics by Ragini *et al.*[43] that such transitions between two ferroelectric phases exhibit pronounced anomalies in the temperature dependence of piezoelectric resonance frequency (f_r) which is a measure of the elastic modulus (E) of the material ($f_r \propto \sqrt{E}$). In view of this, we have used "f_r" measurements to search for the transitions occurring below room temperature. Fig. 4 shows the variation of piezoelectric resonance frequency with temperature below 300 K for the four representative compositions of PMN-xPT with x=0.25, 0.29, 0.32, and 0.36. The compositions with x=0.25, 0.29, and 0.32 behave like normal solids which expand on heating and for which, the elastic modulus, and hence f_r, is expected to increase on cooling from higher temperature side. However, for the composition with x=0.36, f_r decreases with decreasing temperature, shows a minimum around 235 K and then it starts increasing on further lowering of the temperature. The decreasing value of f_r with decreasing temperature up to 235 K is anomalous and is a signature of a lattice instability due to a soft mode for an impending structural phase transition.[43] This anomalous behavior disappears below 235 K as f_r starts increasing with decreasing temperature thereafter, as expected for a normal solid. Thus the soft mode freezes at around 235 K. This clearly reveals a phase transition from the room temperature tetragonal phase to another phase for x=0.36 at 235 K. A similar low temperature phase transition was observed for other tetragonal compositions also in the vicinity of the MPB with x=0.35 and 0.37. Unlike these tetragonal compositions, the temperature dependence of f_r for the room temperature rhombohedral, monoclinic M_B and monoclinic M_C phases of PMN-xPT with x=0.25, 0.29, and 0.32, respectively, do not show any evidence for a low temperature phase transition.

The f_r measurement also indicate a phase transition at the "weak" dielectric anomaly temperature shown in the inset to Fig. 1(b) for x=0.32. This is illustrated in Fig. 5 which depicts the temperature variation of f_r for x=0.32 above room temperature. It is evident that a phase transition does occur at 380±1 K as the sign of the temperature coefficient of f_r changes at this temperature. From the very broad and weak dielectric anomaly shown in the inset to Fig. 1(b), it was not possible to determine this phase transition temperature so precisely (within ±1 K).

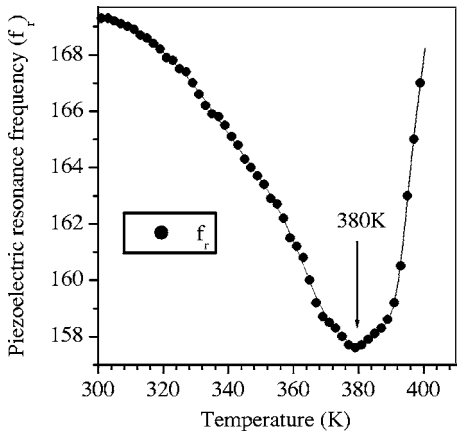

FIG. 5. Variation of piezoelectric resonance frequency (f_r) with temperature above 300 K for PMN-0.32PT ceramics depicting a M_C to tetragonal phase transition around 380 K.

B. Powder neutron diffraction studies

We shall now correlate the anomalies in $\varepsilon(T)$ and $f_r(T)$ with various structural changes using Rietveld analysis of powder neutron diffraction data for $x=0.25$, 0.29, 0.32, and 0.36, representative of the rhombohedral (R), monoclinic M_B, monoclinic M_C, and tetragonal (T) structures at room temperature, respectively. To study the structural changes, we have concentrated on the evolution of the very high angle cubic peaks such as 400, 440, and 620 so that the splittings of the peaks in the lower symmetry phases become discernible.

1. Phase transitions in PMN-0.25PT

The room temperature structure of PMN-xPT is generally believed to be rhombohedral with space group $R3m$ for compositions with $x \leqslant 0.26$.[11] This phase remains stable at low temperatures also as shown in Sec. III A using dielectric and piezoelectric resonance frequency measurements. The rhombohedral PMN-0.25PT ceramics on heating transform into the paraelectric cubic phase above 395 K.

The pseudocubic 400, 440, and 620 neutron powder diffraction profiles recorded at 80 K, 300 K, and 500 K are shown in Fig. 6 along with the Rietveld fits and agreement factors obtained using the entire neutron powder diffraction data in the 2θ range 14 to 155°. At 500 K, each one of the three profiles is a singlet which is consistent with the cubic structure with space group $Pm3m$ and further confirmed by the good match between the observed and calculated patterns [see Fig. 6(a)]. At 300 K, the 440 and 620 profiles get broadened and the 440 profile show clear asymmetry on the lower two θ side indicating a change of crystal structure by lowering the temperature from 500 K to 300 K. The Rietveld refinement of the structure using rhombohedral $R3m$ space group below the transition temperature 395 K, accounts for

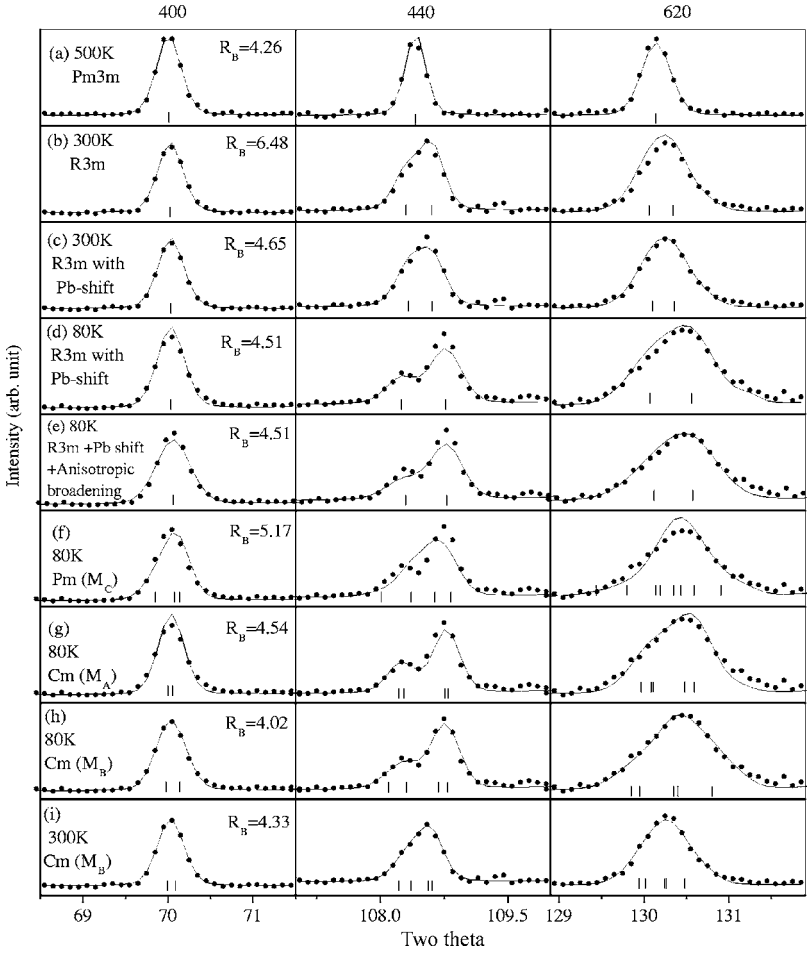

FIG. 6. Evolution of 400, 440, and 620 cubic powder neutron diffraction profiles with temperature for PMN-0.25PT ceramics. The observed data is shown by dots, continuous line shows calculated patterns obtained after Rietveld refinement corresponding to various structural models and the vertical tick marks show the positions of various Bragg reflections.

most of the features of the observed neutron diffraction profiles but the fit between the observed and calculated profiles is not satisfactory as can be seen from Fig. 6(b) for the 620 profile. The agreement factors are also unsatisfactory. Similar intensity mismatch between the observed and calculated profiles have been reported by Corker *et al.*[44] in the case of the rhombohedral phase of PZT and has been attributed to local monoclinic displacements within the global rhombohedral structure.[7] We therefore refined the structure at 300 K considering local ⟨100⟩ displacements of Pb superimposed on the [111] shift of the rhombohedral structure. The rhombohedral structure with local displacements of Pb atom gave considerably lower agreement factors with improvement in the fit between the observed and calculated profiles for reflections like 620 as shown in Fig. 6(c) but the fit for the 440 type profiles has deteriorated. For the 80 K pattern, the rhombohedral structure with local lead shift leads to unsatisfactory fit [see Fig. 6(d)] for all the three reflections shown in the figure. In all these refinements, we assumed isotropic peak broadening function. However, anisotropic peak broadening functions[45] have been used successfully for refining the structure of several Pb based perovskites.[12] Before proposing any lower symmetry structure, we therefore considered anisotropic profile shape function also in our refinements to see if it can account for the large broadening of the 620 profile. As shown in Fig. 6(e), the fit for the 620 profile in fact improves after using anisotropic peak broadening function but the fits for the other reflections such as 440 and 400 profiles deteriorate. As a result, the overall Bragg *R* factor (R_B) does not show any improvement even after considering anisotropic peak broadening.

As the next step, we considered the model of Ragini *et al.*,[8] which has subsequently been corroborated by Glazer *et al.*[46] also. According to this model, the anomalous peak broadening in the so-called rhombohedral compositions of PZT are indeed due to a monoclinic structure with *Cm* space group. In the PMN-*x*PT system, an M_B phase with *Cm* space group has already been confirmed for the composition range $0.27 \leqslant x \leqslant 0.30$,[11] which were also considered to be rhombohedral. In view of this we considered the M_B phase in our refinements for $x < 0.27$ as well. Since there are two other possible monoclinic phases (M_C and M_A type), we considered them also in our refinements for the sake of completeness of the analysis. Out of the three monoclinic M_C, M_A, and M_B phases, the M_B phase gives the lowest *R* factors and good fit between the observed and calculated profiles [see Figs. 6(f)–6(h)]. It is evident from Fig. 6(f) that the monoclinic M_C phase gives very bad fit between the observed and calculated profiles even though it has a larger number of refinable parameters in comparison with the monoclinic M_A and M_B phases. The resulting R_B (5.17) for the monoclinic M_C phase is much higher than even that for the pseudorhombohedral model (R_B=4.51) shown in Fig. 6(d). Thus the monoclinic M_C phase can be easily ruled out. A comparison of Fig. 6(g) with Fig. 6(h) suggests that the fits for the monoclinic M_A phase are inferior to those for the M_B phase with significantly higher *R* factor, even though the number of refinable parameters are identical for both the models. This clearly favors the monoclinic M_B phase over the M_A phase. Since there is no structural phase transition between the room temperature and 80 K for PMN-0.25PT [see Sec. III A], we believe that the monoclinic M_B structure is the correct structure at room temperature also. Consideration of the M_B phase in the refinements indeed gives better fit between the observed and calculated profiles [see Fig. 6(i)], as compared to the rhombohedral structure model considered in Fig. 6(b). We thus conclude that the monoclinic M_B phase, reported earlier to be stable in the composition range $0.27 \leqslant x \leqslant 0.30$ only, exists in the entire composition range $x \leqslant 0.30$.

The question may now arise as to why the M_B phase in the composition range $0.27 \leqslant x \leqslant 0.30$ exhibits peak splittings in the high angle 440 and 620 reflections[26] but not for $x < 0.27$. This has to be attributed to smaller ferroelectric domain sizes for $x < 0.27$ leading to larger Scherrer broadening masking the peak splitting. This explanation is consistent with the experimental observation of decreasing domain size with decreasing Ti-concentration in the PMN-*x*PT system.[19] What is most striking in the 80 K pattern for $x=0.25$ is the large broadening of the 620 profile as compared to the instrumental broadening revealed by the width of the same reflection at 500 K in the cubic phase. For a rhombohedral phase, the 620 peak should have been a doublet but if one tries to fit two peaks, each of width equal to that of the cubic peak at 500 K, there is a clear misfit. One can in principle explain the overall width of the 620 peak using two peaks, each of much larger widths as compared to that of the 620 peak at 500 K. This would imply that the rhombohedral domain size is decreasing with decreasing temperature since the width of the 620 profile increases considerably on lowering the temperature from 300 K to 80 K. But such a decreasing domain size with temperature is physically unrealistic as the ferroelectric ordered regions are known to grow with decreasing temperature. The unusual broadening of the diffraction profiles at low temperatures may also arise due to the coexistence of phases around a first order phase transition temperature. However, there is no phase transition taking place in PMN-0.25PT between 300 K and 80 K [see Sec. III A] and hence the question of the appearance of a second phase below room temperature does not arise. The other standard explanation for the anomalously large broadening at 80 K can be in terms of anisotropic peak broadening due to fluctuations in lattice parameters as per the model of Stephens.[45] Such fluctuations in lattice parameters are usually caused by frozen-in compositional fluctuations but the broadening caused by compositional fluctuations cannot be temperature dependent. Any temperature dependent anisotropic peak broadening has therefore to be attributed to presence of a lower symmetry phase, such as M_B phase in the present case whose monoclinic distortion grows with decreasing temperature as can be seen from Fig. 7.

The dielectric results presented in Sec. III A suggest relaxor ferroelectric behavior for PMN-0.25PT. The observation of a structural change associated with the relaxor type dielectric anomaly may appear somewhat intriguing, as macroscopic symmetry breaking is not observed in the ergodic and nonergodic relaxor ferroelectric phases of pure PMN.[40] However macroscopic symmetry breaking has been reported for the nonergodic relaxor ferroelectric phases of PMN-0.10PT (Ref. 42) below the Vogel-Fulcher freezing tempera-

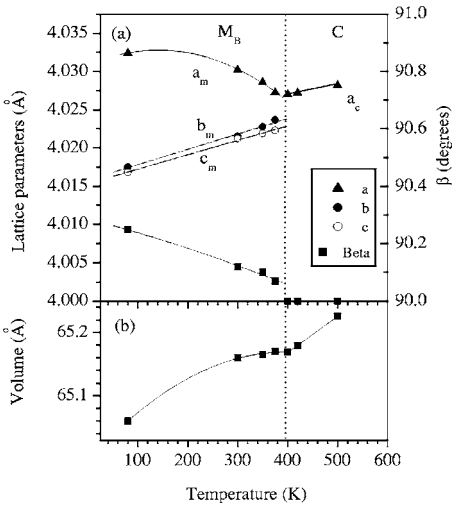

FIG. 7. (a) Evolution of the lattice parameters of the pseudorhombohedral M_B phase with temperature for PMN-0.25PT obtained after Rietveld analysis of neutron powder diffraction data at various temperatures. For easy comparison with the cubic cell parameters, the equivalent perovskite cell parameters a_m and b_m calculated from the monoclinic cell parameters A_m and B_m are plotted ($a_m=A_m/\sqrt{2}$ and $b_m=B_m/\sqrt{2}$). (b) Temperature dependence of the unit cell volume. The error bar for each data point is smaller than the size of the symbols.

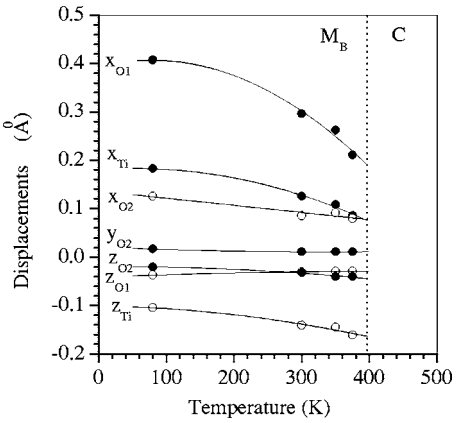

FIG. 8. Variation of the atomic shifts with temperature for PMN-0.25PT as obtained by Rietveld analysis of powder neutron diffraction data. The error bar for each data point is smaller than the size of the symbols.

ture (T_{VF}) of 285 K. In the present case (i.e., for $x=0.25$), the Vogel-Fulcher freezing (381 K) temperature is found to be well above the room temperature and hence the observation of macroscopic symmetry breaking at room temperature, similar to that reported in PMN-0.10PT below T_{VF}, is not unexpected. The fact that a bulk diffraction probe such as neutron diffraction reveals symmetry breaking suggests that the size of the polar regions of PMN has increased substantially as a result of $PbTiO_3$ substitution. Similar to PMN-0.25PT and PMN-0.10PT, pure PMN also exhibits nonergodic relaxor ferroelectric phase below T_{VF} but the size of the polar regions is not big enough to show characteristic splitting of powder diffraction peaks. The observation of a hard mode below T_{VF} in PMN by Wakimoto *et al.*[47] suggests that the nonergodic relaxor ferroelectric phase is similar to the normal ferroelectric phase in lattice dynamical sense.

The evolution of the lattice parameters with temperature for PMN-0.25PT obtained after Rietveld analysis of neutron powder diffraction data at various temperatures is depicted in Fig. 7. For easy comparison with the cell parameter of the cubic (a_C) phase, the equivalent perovskite cell parameters a_m and b_m, which are related to the monoclinic A_m and B_m cell parameters as $A_m/\sqrt{2}$ and $B_m/\sqrt{2}$, are shown in this figure. It is evident from this figure that the monoclinic angle β decreases linearly with increasing temperature. The values of b_m and Cm cell parameters are very close and increase linearly with temperature upto the Curie point whereas a_m decreases continuously with increasing temperature. At the Curie point there is a discontinuous change in b_m, Cm and β but not in a_m.

In normal ferroelectric oxides, the unit cell volume decreases linearly on cooling up to the Curie point and then increases in the ferroelectric transition region due to the displacement of ions. It, however, again decreases with temperature on further cooling because of the dominance of the thermal contraction effects. In relaxors, in contrast, the presence of polar nanoregions generates dilatational electrostrictive strain[40] which offsets the thermal contraction behavior to such an extent that the cell volume becomes nearly temperature independent in the Curie range.[48] In PMN-0.25PT, we find that the unit cell volume is nearly constant in the temperature range 400 K to 300 K [see Fig. 7(b)] which mimics relaxor like features.

Figure 8 shows the variation of atomic shifts (δ) with temperature for PMN-0.25PT for the M_B phase. The y_{O2}, z_{O2}, and z_{O1} displacements are rather small in magnitude and are almost constant over the entire temperature range below T_m'. The largest displacement is observed for x_{O1}, followed by x_{Ti}, z_{Ti}, and x_{O2}. The x_{O1} shift decreases at the fastest rate and becomes zero discontinuously at the $R3m$ to $Pm3m$ phase transition temperature. Based on the observation of thermal hysteresis in the optical birefringence, Zekria and Glazer[49] have proposed a first order transition between the ferroelectric and paraelectric cubic phases for compositions with $x<0.30$. The discontinuous change of several microscopic order parameters ($x_{Ti}, z_{Ti}, x_{O2}, x_{O1}$) at the transition temperature seems to favor a first order structural phase transition even though the unit cell volume discontinuity is smoothened out due to the electrostrictive strains caused by polar regions. The refined structural parameters for PMN-0.25PT at various temperatures are listed in Table I.

2. Phase transitions in PMN-0.29PT

Figure 9 shows the evolution of 400, 440, and 620 pseudocubic profiles as a function of temperature for PMN-0.29PT. At 500 K all the three profiles are singlet as expected for the cubic phase [Fig. 9(a)]. The cubic structure at 500 K is consistent with the results of the high temperature dielectric measurements also which give $T_m' \approx 419$ K at 1 kHz. In the data for 415 K [Fig. 9(b)], which is just below the Curie point, the 620 profile has split whereas the 440 profile shows an asymmetric tail on the higher 2θ side and 400 profile

TABLE I. Refined structural parameters for PMN-0.25PT at different temperatures.

Structure (S.G.)	Monoclinic (*Cm*)				Cubic (*Pm*3*m*)		
Temp. (K)	80	300	350	375	400	450	500
a (Å)	5.7022(3)	5.6987(5)	5.6969(6)	5.6952(9)	4.0242(1)	4.0244(1)	4.02545(1)
b (Å)	5.6815(4)	5.687(6)	5.6889(5)	5.6903(8)	—	—	—
c (Å)	4.0167(3)	4.0211(4)	4.0215(1)	4.0220(1)	—	—	—
β (°)	90.248(5)	90.135(8)	90.109(1)	90.083(1)	—	—	—
β_{11}(Pb)	0.007(1)	0.014(1)	0.019(2)	0.024(4)			
β_{22}(Pb)	0.027(1)	0.032(2)	0.032(3)	0.031(4)	3.994(4)	3.98(4)	3.92(4)
β_{33}(Pb)	0.038(2)	0.036(4)	0.037(5)	0.035(4)			
β_{13}(Pb)	0.009(1)	0.011(1)	0.011(2)	0.010(3)			
$X_{\text{Ti/Nb/Mg}}$	0.532(1)	0.522(1)	0.519(2)	0.515(2)	—	—	—
$Z_{\text{Ti/Nb/Mg}}$	0.474(2)	0.465(4)	0.464(4)	0.460(4)	—	—	—
B(Ti/Nb/Mg)	0.37(3)	0.41(4)	0.43(4)	0.39(6)	0.38(2)	0.49(2)	0.62(2)
X_{O1}	0.5714(9)	0.552(1)	0.546(2)	0.537(2)	—	—	—
Z_{O1}	−0.037(2)	−0.030(4)	−0.029(4)	−0.029(5)	—	—	—
B(O1)	0.73(4)	1.16(9)	1.4(1)	1.4(2)	1.67(1)	1.63(1)	1.64(1)
X_{O2}	0.272(1)	0.265(2)	0.266(3)	0.264(5)	—	—	—
Y_{O2}	0.2530(6)	0.252(1)	0.252(1)	0.252(2)	—	—	—
Z_{O2}	0.495(2)	0.492(4)	0.490(4)	0.490(5)	—	—	—
B(O2)	0.85(2)	1.28(5)	1.40(7)	1.5(1)	—	—	—
R_{wp}	7.46	6.93	7.09	7.73	9.32	9.05	7.64
R_{exp}	3.02	3.13	3.20	3.21	3.23	3.19	3.08
χ^2	6.10	4.90	4.90	4.79	8.32	8.04	6.15

shows asymmetry on the lower 2θ side. All these features are consistent with the tetragonal structure with $P4mm$ space group. Due to small tetragonal distortion at higher temperatures, splitting of the 400 and 440 cubic peaks into a pair of peaks with indices 004/400 and 404/440, respectively, is not clearly seen except through the presence of the asymmetries in the tails. However, the high angle 620 peak does show clear splitting consistent with the tetragonal structure. Rietveld analysis of the entire diffraction pattern in the 2θ range 14 to 155° confirms a tetragonal structure of PMN-0.29PT at 415 K with space group $P4mm$ as can be seen from the satisfactory fit between the observed and calculated profiles shown in Fig. 9(b). The tetragonal phase of PMN-0.29PT undergoes a further phase transition as can be seen from a comparison of the profile shapes at 300 K [Fig. 9(c)] and 80 K [Fig. 9(d)] with those at 415 K. The asymmetric tail of the 440 profile, present on the higher 2θ side in the 415 K pattern shown in Fig. 9(b), appears now on the lower

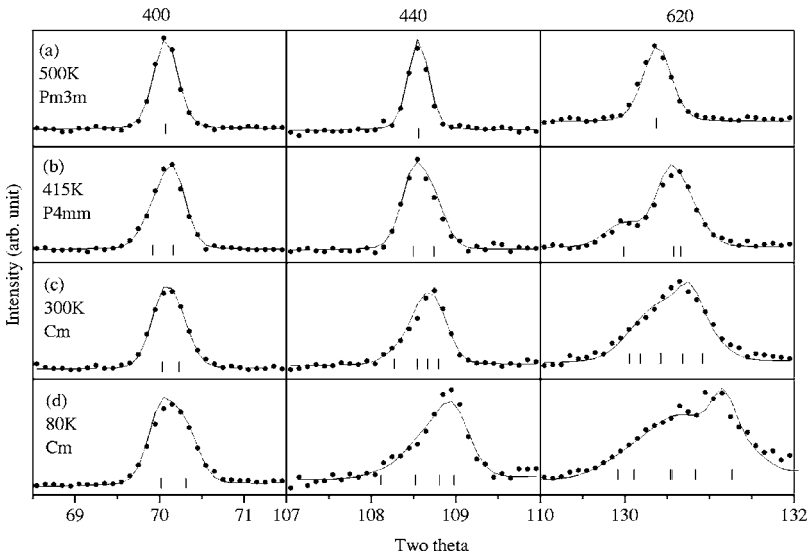

FIG. 9. Evolution of the 400, 440, and 620 cubic powder neutron diffraction profiles as a function of temperature for PMN-0.29PT. The solid dots show the observed diffraction profiles, while the continuous line the calculated patterns obtained by the Rietveld analysis of the neutron powder diffraction data for different structures. The vertical tick marks show the positions of various Bragg reflections.

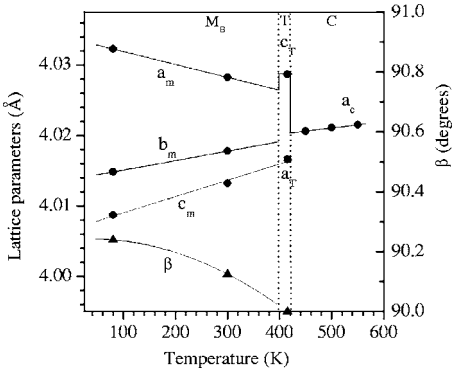

FIG. 10. Evolution of the lattice parameters with temperature for PMN-0.29PT obtained after Rietveld analysis of the neutron powder diffraction data at various temperatures. For easy comparison, the equivalent perovskite cell parameters a_m and b_m calculated from the monoclinic cell parameters A_m and B_m, are plotted in the monoclinic region ($a_m=A_m/\sqrt{2}$, $b_m=B_m/\sqrt{2}$). The error bar for each data point is smaller than the size of the symbols.

2θ side in Figs. 9(c) and 9(d). This may at first instance suggest a rhombohedral structure at 300 K and 80 K. However, if it were a rhombohedral phase, the 400 peak should have been a singlet. The large broadening of the 400 profile at 300 K, as compared to the width of the same profile in the cubic phase, i.e., at 500 K, clearly indicates the presence of more than one peak. In addition, the 620 profile should have consisted of two sharp components for the rhombohedral structure. But the overall FWHM of this profile is much more than the sum of two resolution limited peaks. All these features rule out the rhombohedral structure for PMN-0.29PT at 300 K and 80 K. As already shown elsewhere[26] using detailed analysis of powder neutron diffraction data, the structure of PMN-0.29PT is monoclinic with *Cm* space group of M_B type at room temperature (300 K). This is further corroborated by the good fit between the observed and calculated profiles for 300 K and 80 K obtained by Rietveld analysis using *Cm* space group (see Fig. 9). It also confirms the absence of any low temperature phase occurring below 300 K in PMN-0.29PT in agreement with the dielectric and piezoelectric resonance frequency measurements reported in Sec. III A.

The evolution of the lattice parameters with temperature for PMN-0.29PT is depicted in Fig. 10. For easy comparison with the cell parameters of the tetragonal (a_T, c_T) and cubic (a_C) phases, the equivalent perovskite cell parameters a_m and b_m, which are related to the true monoclinic A_m and B_m cell parameters as $A_m/\sqrt{2}$ and $B_m/\sqrt{2}$, are plotted in the monoclinic region. The orientation relationship between monoclinic and tetragonal cells is such that $[110]_m \| [100]_T$, $[1\bar{1}0]_m \| [010]_T$ and $[001]_m \| [100]_T$. It is evident from this figure that the *Cm* cell parameter becomes equal to a_T parameter of the tetragonal phase continuously whereas the b_m parameter approaches a_T discontinuously at the monoclinic to tetragonal phase transition temperature. The a_m parameter decreases with increasing temperature but shows a discontinuous jump to become c_T at the monoclinic to tetragonal

TABLE II. Refined structural parameters for PMN-0.29PT at different temperatures.

Structure (S.G.)	Monoclinic (Cm)		Tetragonal (*P*4*mm*)	Cubic (*Pm*3*m*)		
Temp. (K)	80	300	415	450	500	550
a (Å)	5.7025(3)	5.6968(3)	4.0166(1)	4.0206(1)	4.0211(1)	4.0215(1)
b (Å)	5.6778(3)	5.6820(4)				
c (Å)	4.0087(2)	4.0132(3)	4.0287(2)			
β (°)	90.240(6)	90.125(8)				
β_{11}(Pb)	0.0089(9)	0.0070(8)	3.75(5)	3.86(4)	3.89(4)	3.86(4)
β_{22}(Pb)	0.027(1)	0.030(2)				
β_{33}(Pb)	0.034(2)	0.051(3)				
$X_{\text{Ti/Nb/Mg}}$	0.5351(9)	0.530(1)				
$Z_{\text{Ti/Nb/Mg}}$	0.484(2)	0.500(6)	0.521(1)			
B(Ti/Nb/Mg)	0.35(3)	0.63(6)	0.45(3)	0.46(2)	0.61(2)	0.65(2)
X_{O1}	0.5727(8)	0.536(1)				
Z_{O1}	−0.030(2)	−0.009(5)	0.038(1)			
B(O1)	0.55(4)	1.0(1)	1.8(1)	1.65(1)	1.64(1)	1.67(1)
X_{O2}	0.270(1)	0.295(1)				
Y_{O2}	0.2524(6)	0.258(1)				
Z_{O2}	0.498(2)	0.481(4)	0.5495(9)			
B(O2)	0.87(3)	1.42(7)	1.25(3)			
R_{wp}	8.25	8.01	6.78	9.04	7.75	7.50
R_{exp}	3.07	3.37	3.22	3.38	3.27	3.23
χ^2	7.22	5.64	4.43	7.15	5.61	5.39

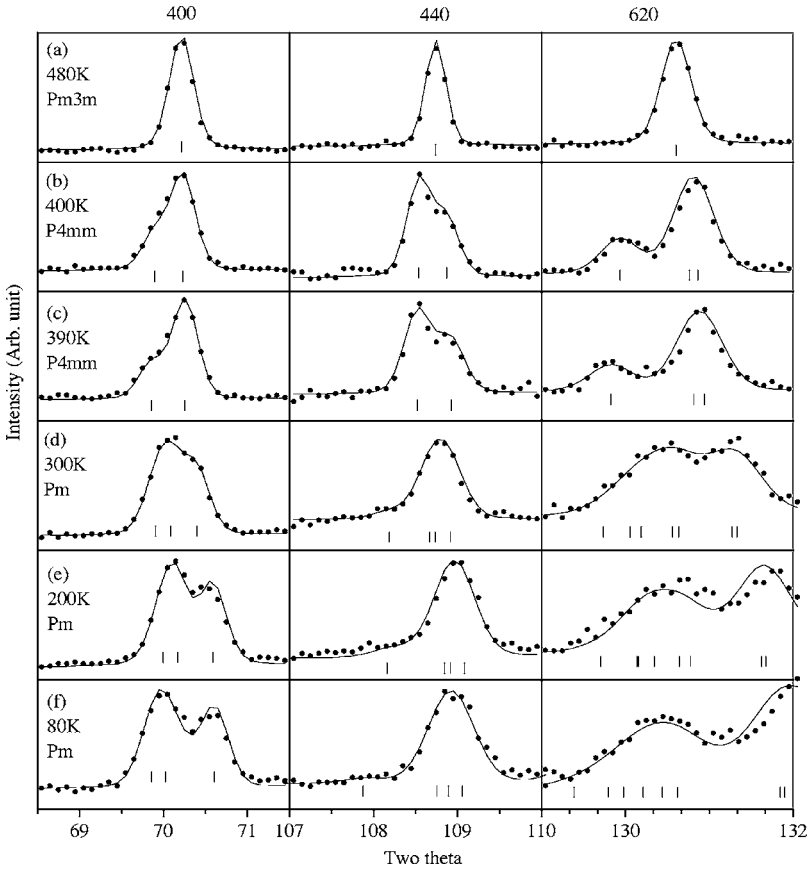

FIG. 11. Evolution of the 400, 440, and 620 cubic powder neutron diffraction profiles for *PM*N-0.32PT as a function of temperature. The solid dots show the observed diffraction profiles, while the continuous line the calculated patterns obtained by the Rietveld analysis of the neutron powder diffraction data for various structures. The vertical tick marks show the positions of various Bragg reflections.

phase transition temperature. It is worth mentioning that Noheda *et al.*[24] have analyzed a neighboring composition, PMN-0.30PT using rhombohedral structure at room temperature and below. Our results presented in Figs. 9 and 10 do not favor the rhombohedral structure for the composition range $x \leqslant 0.30$ and suggest the existence of a monoclinic *Cm* phase of M_B type. The refined structural parameters for PMN-0.29PT at different temperatures are given in Table II.

In the piezoelectric resonance frequency measurements, we have found clear signature of one more transition between the room temperature monoclinic and the high temperature tetragonal phase for compositions with $0.27 \leqslant x \leqslant 0.30$. Rietveld analysis of the powder neutron diffraction data at $T=380$ K confirms that the room temperature monoclinic *Cm* phase transforms into the tetragonal phase via the monoclinic *Pm* phase. The intermediate *Pm* phase is observed due to the tilted nature of the *Cm*-*Pm* phase boundary similar to *Pm*-*P*4*mm* phase boundary. The three anomalies recently observed in the dielectric measurements on single crystals of PMN-*x*PT ($x=0.295$ and 0.30) could also be due to such a sequence of phase transition from the monoclinic *Cm* to monoclinic *Pm* and then to the tetragonal structure which finally transforms to the cubic phase.[50,51]

Lu *et al.*[52] have also reported a succession of three transitions above room temperature using dielectric measurements on a PMN-0.33PT crystal. They have attributed these transitions to changes from rhombohedral to orthorhombic to tetragonal to cubic structures. We do not find any evidence for these transitions in PMN-0.33PT samples. However, the room temperature structure of PMN-*x*PT for $x=0.33$ is known to be monoclinic M_C type[11,24] and not rhombohedral considered by Lu *et al.*[52] The Curie point (433 K) for PMN-0.33PT is also found to be quite different from that (418 K) reported by Lu *et al.*[52] The composition dependence of the Curie point shown in Fig. 2 suggests that a Curie point of 418 K corresponds to the composition $x=0.29$. We therefore believe that the correct composition of the crystals used by Lu *et al.*[52] may be different from the nominal composition and may be close to $x=0.29$ for which we also observe pseudorhombohedral nature of diffraction profiles at room temperature and a succession of three transitions similar to that reported by Lu *et al.*[52] Based on the structural studies pre-

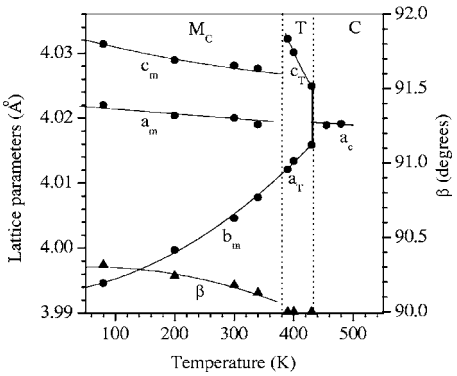

FIG. 12. Evolution of the lattice parameters with temperature for PMN-0.32PT obtained after Rietveld refinement of neutron powder diffraction data at various temperatures. The error bar for each data point is smaller than the size of the symbols.

TABLE III. (Top) Refined structural parameters for monoclinic PMN-0.32PT at different temperatures. (Bottom) Refined structural parameters for tetragonal and cubic PMN-0.32PT at different temperatures.

Structure (S.G.)	Monoclinic phase (Pm)			
Temp. (K)	80	200	300	340
a (Å)	4.0220(4)	4.0204(4)	4.0200(3)	4.0190(2)
b (Å)	3.9946(2)	3.9997(2)	4.0046(2)	4.0078(2)
c (Å)	4.0314(4)	4.0289(4)	4.0281(3)	4.0276(2)
β (°)	90.314(5)	90.241(4)	90.178(5)	90.128(6)
B_{iso}(Pb)	2.52(6)	2.51(6)	2.91(1)	3.01(6)
$X_{Ti/Nb/Mg}$	0.474(3)	0.465(3)	0.472(3)	0.460(3)
Z_{Ti}	0.550(2)	0.545(2)	0.533(2)	0.525(2)
B(Ti/Nb/Mg)	0.18(5)	0.19(5)	0.40(5)	0.24(6)
X_{O1}	0.503(2)	0.497(2)	0.496(2)	0.493(2)
Z_{O1}	0.530(2)	0.524(2)	0.519(2)	0.517(2)
B(O1)	0.68(6)	0.60(5)	0.84(5)	1.0(7)
X_{O2}	0.510(3)	0.507(4)	0.504(4)	0.491(3)
Z_{O2}	0.019(3)	0.009(4)	0.007(4)	0.003(3)
B(O2)	1.02(8)	1.27(8)	1.39(9)	1.4(1)
X_{O3}	–0.047(2)	–0.046(2)	–0.036(2)	–0.034(2)
Z_{O3}	0.584(2)	0.579(2)	0.572(2)	0.566(2)
B(O3)	0.53(6)	0.71(6)	1.01(8)	1.2(1)
R_{wp}	8.08	8.09	6.77	6.82
R_{exp}	3.03	3.03	3.06	3.25
χ^2	7.11	7.12	4.89	4.40

Structure (S.G.)	Tetragonal ($P4mm$)			Cubic ($Pm3m$)	
Temp. (K)	390	400	430	455	480
a (Å)	4.0121(1)	4.0134(1)	4.0159(1)	4.0189(1)	4.0191(1)
c (Å)	4.0322(2)	4.0301(2)	4.0249(2)		
B_{iso}(Pb)	3.35(5)	3.53(5)	3.74(6)	3.83(4)	3.8(4)
$Z_{Ti/Nb/Mg}$	0.529(1)	0.525(1)	0.517(1)		
B(Ti/Nb/Mg)	0.33(3)	0.33(3)	0.54(3)	0.45(2)	0.6(2)
Z_{O1}	0.049(1)	0.044(1)	0.031(2)		
B(O1)	1.72(8)	1.84(9)	1.7(1)	1.64(1)	1.67(1)
Z_{O2}	0.5597(8)	0.5541(8)	0.543(1)		
B(O2)	1.22(3)	1.23(3)	1.37(5)		
R_{wp}	7.72	7.51	7.26	8.66	7.56
R_{exp}	3.25	3.23	3.22	3.17	3.13
χ^2	5.64	5.40	5.08	7.46	5.83

sented in this work, the most likely sequence of structural changes associated with the three transitions reported by Lu *et al.*[52] is monoclinic M_B to monoclinic M_C, monoclinic M_C to tetragonal and tetragonal to cubic. The so-called rhombohedral phase of Lu *et al.*[52] may in fact be the M_B phase whereas the intermediate orthorhombic phase reported by these workers may correspond to M_C phase in the limit of β becoming 90°.

The results presented in the previous and the present sections *suggest* that the space group of PMN-xPT at room temperature for the composition ranges $x<0.27$ as well as $0.27\leqslant x\leqslant 0.30$ is Cm. However, there are important differences between these two composition ranges. For the compositions with $x<0.27$, the local displacements of the Pb ion along ⟨110⟩ pseudocubic direction is so small that the average structure mimics pseudorhombohhedral features at room temperature. On lowering the temperature, the local displacements progressively increase enabling a choice to be made between the $R3m$ and Cm space groups at low temperatures (see, e.g., the fits at 80 K in Fig. 6). For the composition

range $0.27 \leqslant x \leqslant 0.30$, the monoclinic distortion is large enough to be distinguished easily from the rhombohedral distortion even at room temperature. This implies that the effect of lowering the temperature in bringing out the characteristic features of *Cm* space group for $x < 0.27$ is equivalent to the effect of increasing x beyond 0.27 at room temperature. The difference in the monoclinic distortion at room temperature in the two composition ranges may be due to the difference in the structure of the high temperature phase from which the *Cm* phase has originated. The pseudorhombohedral phase of PMN-xPT with $x < 0.27$ originates directly from the paraelectric cubic phase whereas the monoclinic *Cm* phase for $0.27 \leqslant x \leqslant 0.30$ originates from the tetragonal/monoclinic *Pm* phases. The absence of a peak at $x \approx 0.27$ in the variation of the dielectric constant[11] and d_{33} (Ref. 31) with composition, corresponding to the rhombohedral-M_B phase boundary reported in Ref. 11, may also be rationalized in terms of the presence of M_B type local order in the pseudorhombohedral compositions with $x < 0.27$. Since there is no change of symmetry at $x=0.27$, one does not expect a peak in the composition dependence of dielectric constant and d_{33} at room temperature in agreement with the experimental observations.[11,31] In case of the rhombohedral structure for $x < 0.27$, one would expect a peak in dielectric constant and d_{33} at $x=0.27$ similar to the peaks reported in literature[11,31] at $x=0.30$ and 0.35 corresponding to the M_B-M_C and the M_C-tetragonal phase boundaries.

3. Phase transitions in PM-0.32PT

The paraelectric to ferroelectric transition in PMN-0.32PT occurs around 433 K [see Fig. 1(b)]. The structure of the paraelectric phase is cubic above this temperature as can bee seen from the singlet nature of the 400, 440, and 620 profiles at 480 K [see Fig. 11(a)]. On cooling below 433 K, the structure becomes tetragonal as evidenced by the splittting of the 400, 440 and 620 cubic peaks in the pattern recorded at 400 K and 390 K [see Figs. 11(b) and 11(c)]. The 400 profile has become a doublet at 400 K and 390 K with the weaker reflection occurring on the lower 2θ side. The 440 profile is also a doublet but with the weaker reflection occurring on the higher 2θ side. Further, the 620 profile is a well split doublet. Such profile splittings are expected for the tetragonal phase. Strictly speaking, the 620 profile for the tetragonal structure consists of three reflections, viz. 026, 620, and 602. However, the 620 and 602 nearly overlap with each other while 026 occurs towards lower 2θ side which give it a doubletlike appearance. Rietveld analysis of the entire diffraction pattern in the 2θ range 14 to 155° confirms a pure tetragonal structure at 390 and 400 K as indicated by the good fits between the observed and calculated profiles shown in Figs. 11(b) and 11(c). The dielectric data presented in Fig. 1(b) indicates another phase transition around 380 K which was confirmed in our diffraction studies. Thus, for example, the shape of the profiles at 300 K shown in Fig. 11(d) is markedly different from that at 390 K. At 300 K, the weaker reflection appears on the higher 2θ side of the 400 pseudocubic profile in contrast to that observed at 390 K, where it occurs on the lower 2θ side. The higher angle shoulder in the 440 pseudocubic profile of the tetragonal phase at 390 K has also disappeared

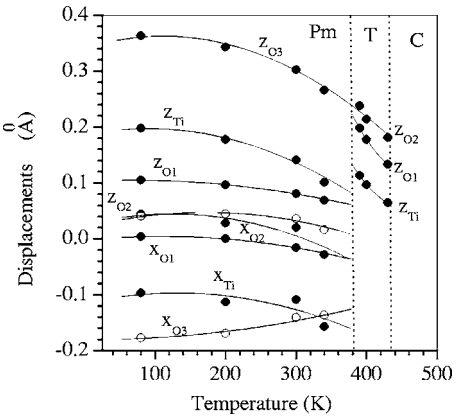

FIG. 13. Variation of the atomic shifts with temperature in the monoclinic and tetragonal phase regions for PMN-0.32PT obtained after Rietveld analysis of powder neutron diffraction data. The error bar for each data point is smaller than the size of the symbols.

in the 300 K pattern whereas the 620 pseudocubic profile has undergone a drastic change in terms of the relative intensities of the two clearly resolvable peaks. All these features clearly indicate a nontetragonal structure at 300 K. On further cooling below the room temperature, the diffraction profiles do not show any additional change, except for the increase in the separation of the two peaks of the 400 profile and a slight lowering of the intensity of the lower angle side peak in the 620 profile. Rietveld analysis of the entire diffraction pattern in the 2θ range 14 to 155° at 300 K $\leqslant T \leqslant$ 80 K shows that a monoclinic phase with *Pm* space group can explain all the observed features of the diffraction pattern. The good Rietveld fits shown in Figs. 11(d)–11(f) for $T \leqslant 300$ K corroborate this. Consideration of a small amount of coexisting tetragonal phase improves the fits between the observed and calculated profiles further and this coexistence is found to persist down to 80 K. The peak positions corresponding to the minority tetragonal phase are not shown in Fig. 11 because its fraction is very small (less than 10%). Noheda *et al.*[24] have also reported a similar coexistence of a minority tetragonal phase in case of PMN-0.33PT that remains untransformed down to the lowest temperatures.

Figure 12 shows the evolution of the lattice parameters with temperature for PMN-0.32PT obtained after Rietveld refinement of neutron powder diffraction data at various temperatures. The b_m cell parameter changes continuously to a_T while a_m changes to a_T discontinuously. The *Cm* cell parameter also changes discontinuously to c_T. Further, the a_T and c_T parameters change discontinuously to a_c. The discontinuous change of lattice parameters observed at the *Pm* to *P*4*mm* and *P*4*mm* to *Pm*3*m* transition temperatures indicate first order nature of these transitions. The similarity of the temperature dependence of the cell parameters for $x=0.32$ with that reported by Noheda *et al.*[24] for $x=0.33$ using synchrotron data is worth noting. The refined cell parameters and positional coordinates of PMN-0.32PT at different temperatures are given in Table III.

We have determined the atomic shifts for various cations and anions in the asymmetric unit of the monoclinic and tetragonal phases at various temperatures. The temperature

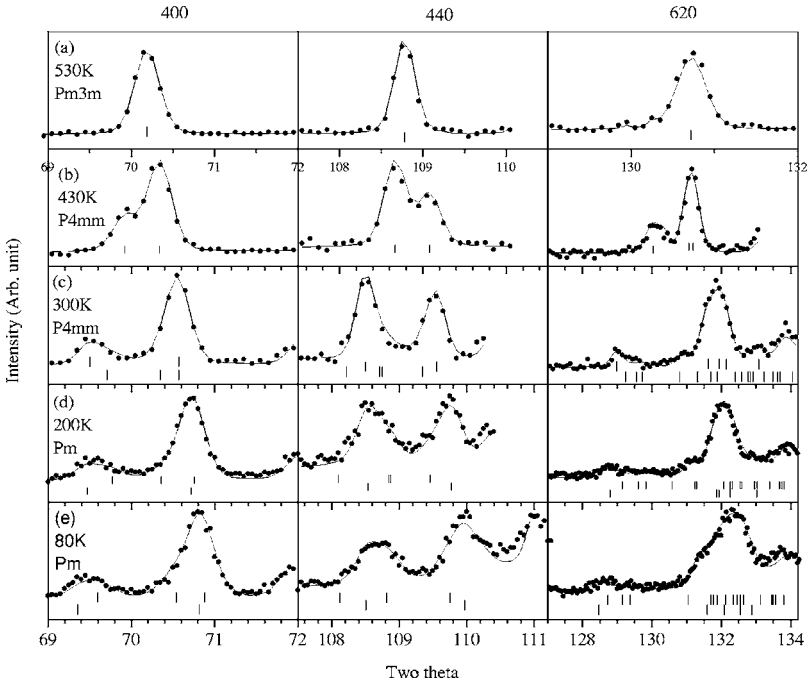

FIG. 14. Evolution of cubic 400, 440, and 620 powder neutron diffraction profiles with temperature for PMN-0.36PT ceramics. The solid dots show the observed diffraction profiles, while the continuous line the calculated patterns obtained by the Rietveld analysis of the neutron powder diffraction data corresponding to various structures. The vertical tick marks show the positions of various Bragg reflections. The scale of the x axis is different for 530 K pattern.

variations of these shifts are shown in Fig. 13. The z_{O3} shift of the *Pm* phase varies continuously across the *Pm* to *P*4*mm* transition temperature but all other parameters exhibit discontinuous changes at this temperature. The *P*4*mm* to *Pm*3*m* transition is also accompanied with discontinuous change of Ti and O positions. All these observations point towards first-order nature of the two transitions. Optical studies on PMN-xPT single crystal by Zekria and Glazer[49] also indicate first order character of *Pm*-*P*4*mm* transition, consistent with our findings. However, this is not consistent with the theoretically predicted phase diagram of Vanderbilt and Cohen[22] which suggests second-order nature of the *Pm*-*P*4*mm* phase boundary on the basis of the eighth-order expansion Landau free energy functional.[22] Consideration of free energy terms up to twelfth order in the phenomenological Landau theory can explain the first-order character of the *Pm* to *P*4*mm* phase transition.[53]

4. Phase transitions in PMN-0.36PT

Figure 14 shows the evolution of the cubic 400, 440, and 620 powder neutron diffraction profiles with temperature. It is evident from this figure that at 530 K [Fig. 14(a)], the structure is cubic since all the 400, 440, and 620 profiles are singlet. This is in agreement with the dielectric measurements also which gives a ferroelectric transition temperature of 449 K for PMN-0.36PT [see Fig. 1(a)]. Below this transition temperature the 400 profile splits into two peaks one of which is weaker and occurs on the lower 2θ side [see Fig. 14(b)]. The 440 profile also becomes a doublet with the weaker reflection occurring on the higher 2θ side. In addition, the 620 profile also shows a doublet appearance. As discussed in the previous section, all these features are consistent with the tetragonal structure. Rietveld analysis of the entire diffraction pattern further confirmed the pure tetragonal structure of PMN-0.36PT at 430 K since the fit between calculated and observed intensities is very good [see Fig. 14(b)]. At 300 K [Fig. 14(c)], the nature of the neutron diffraction profiles is found to be similar to that at 430 K indicating continuation of the tetragonal structure at room temperature also. The splitting of the profiles has increased due to increased tetragonal distortion on lowering the temperature. However, the width of the various reflections has also increased in the 300 K patterns which may be attributed to the presence of a minority coexisting phase. Rietveld refinement of the structure at 300 K confirms the coexistence of minority monoclinic *Pm* phase ($\sim$30%) at room temperature. As a result of this phase coexistence, the intensity of the 404 and 400 peaks has become comparable at 300 K whereas for the pure tetragonal phase they bear approximately 2:1 ratio.

Rietveld analysis of the diffraction data at 200 K reveals that the molar fraction of the monoclinic phase with *Pm* space group has increased to $\sim$53%, i.e., the monoclinic

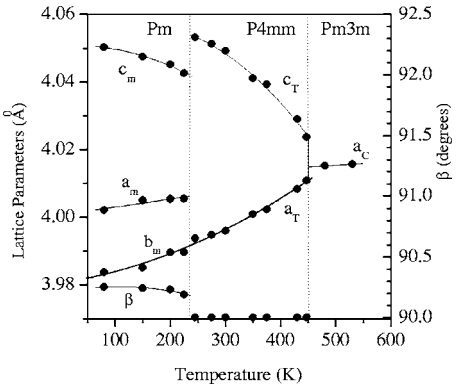

FIG. 15. Evolution of the lattice parameters with temperature for PMN-0.36PT obtained after Rietveld refinement of neutron powder diffraction data at various temperatures. The error bar for each data point is smaller than the size of the symbols.

TABLE IV. (Top) Refined structural parameters for monoclinic PMN-0.36PT at different temperatures. (Bottom) Refined structural parameters for tetragonal and cubic phases of P*M*N-0.36PT at different temperatures.

Structure (S.G.)	Monoclinic phase (*Pm*)			
Temp. (K)	80	150	200	225
a (Å)	4.0022(2)	4.0050(2)	4.0054(6)	4.0055(9)
b (Å)	3.9838(2)	3.9851(2)	3.9896(5)	3.9897(8)
c (Å)	4.0503(2)	4.0475(2)	4.0452(6)	4.0426(8)
β (°)	90.252(4)	90.241(4)	90.23(1)	90.19(2)
B_{iso}(Pb)	2.75(8)	2.92(9)	3.4(1)	3.7(2)
$X_{Ti/Nb/Mg}$	0.462(2)	0.469(3)	0.461(3)	0.471(7)
$Z_{Ti/Nb/Mg}$	0.537(2)	0.532(3)	0.525(4)	0.531(6)
B(Ti/Nb/Mg)	0.13(8)	0.27(9)	0.0(1)	0.2(2)
X_{O1}	0.492(2)	0.499(2)	0.497(2)	0.505(5)
Z_{O1}	0.516(2)	0.519(3)	0.506(3)	0.509(5)
B(O1)	0.86(7)	0.90(9)	0.6(1)	0.7(2)
X_{O2}	0.482(2)	0.496(3)	0.515(3)	0.515(6)
Z_{O2}	0.001(3)	0.003(4)	–0.004(6)	0.001(3)
B(O2)	0.89(7)	1.4(1)	1.2(1)	1.7(2)
X_{O3}	–0.043(1)	–0.039(2)	–0.042(2)	–0.029(5)
Z_{O3}	0.581(2)	0.578(2)	0.571(3)	0.569(5)
B(O3)	0.43(7)	0.20(6)	0.4(1)	0.5(2)
R_{wp}	10.03	9.54	8.30	7.88
R_{exp}	4.23	4.23	4.30	4.38
χ^2	5.62	5.08	3.75	3.23

Structure (S.G.)	Tetragonal phase (*P*4*mm*)							Cubic (*Pm*3*m*)	
Temp. (K)	245	275	300	350	375	430	445	480	530
a (Å)	3.9938(1)	3.9948(1)	3.9960(1)	4.0010(1)	4.0024(1)	4.0083(2)	4.0108(1)	4.0152(1)	4.0157(1)
c (Å)	4.0532(1)	4.0513(2)	4.0492(2)	4.0411(2)	4.0393(1)	4.0290(2)	4.0237(2)		
B_{iso}(Pb)	2.14(6)	2.19(8)	2.3(1)	2.90(5)	2.96(5)	3.46(6)	3.67(7)	3.71(4)	3.74(4)
$Z_{Ti/Nb/Mg}$	0.546(1)	0.545(1)	0.542(1)	0.5373(9)	0.536(1)	0.526(1)	0.515(1)		
$B_{(Ti/Nb/Mg)}$	0.35(6)	0.42(9)	0.48(9)	0.22(3)	0.30(3)	0.50(3)	0.44(4)	0.44(2)	0.53(3)
Z_{O1}	0.072(1)	0.069(1)	0.063(1)	0.059(1)	0.057(1)	0.043(1)	0.036(1)		
B(O1)	1.11(5)	0.99(7)	1.10(7)	1.23(5)	1.27(5)	1.45(8)	1.6(1)	1.64(1)	1.64(1)
Z_{O2}	0.5867(1)	0.584(1)	0.578	0.5711(7)	0.5679(7)	0.5533(8)	0.543(1)		
B(O2)	1.02(3)	1.05(5)	1.16(5)	1.19(3)	1.26(3)	1.37(4)	1.32(4)		
R_{wp}	8.68	7.93	8.77	8.47	8.32	7.91	8.57	7.36	7.27
R_{exp}	3.05	3.10	3.10	3.44	3.42	3.40	3.40	3.18	3.18

phase has now become the majority phase [Fig. 14(d)]. This suggests that a *P*4*mm* to *Pm* transition has occurred between 300 K and 200 K as expected on the basis of the piezoelectric resonance frequency measurements which indicate a phase transition at 235 K (see Fig. 4). On lowering the temperature from 300 K to 80 K the relative intensity of the two broad profiles with the 440 pseudocubic indices changes again. This is due to further reduction of the tetragonal phase fraction on lowering the temperature. Rietveld analysis of the entire diffraction data at 80 K shows that the molar fraction of the monoclinic phase has increased from 53% at 200 K to 63% at 80 K while the minority coexisting tetragonal phase fraction has decreased. Thus the high temperature paraelectric cubic phase first transforms into the tetragonal phase which further transforms into monoclinic phase with *Pm* space group below the room temperature.

The evolution of the lattice parameters with temperature for PMN-0.36PT obtained after Rietveld refinement of neutron powder diffraction data at several temperatures is given in Fig. 15. It is evident from this figure that the monoclinic cell parameter b_m merges with the a_T parameter of the tetragonal phase continuously. The a_m and the *Cm* parameters of

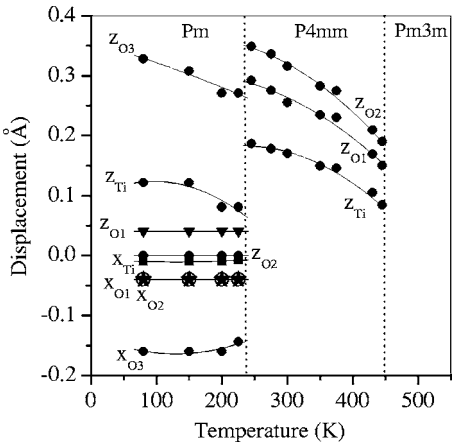

FIG. 16. Variation of the atomic shifts with temperature in the monoclinic and tetragonal phase regions for PMN-0.36PT ceramics. The error bar for each data point is smaller than the size of the symbols.

the monoclinic *Pm* phase, on the other hand, change discontinuously at the *Pm* to *P*4*mm* phase transition temperature. The variation of the cell parameters shown in Fig. 15 are similar to that reported by Noheda *et al.*[24] for the tetragonal compositions with $x=0.37$. At the *P*4*mm*-*Pm*3*m* phase boundary, a discontinuous change of cell parameters is observed which indicates that this phase boundary is of first-order. It is interesting to note that the variation of cell parameters with temperature are similar to that observed for PMN-0.32PT (see Fig. 12) except for the wider stability region of the tetragonal phase. The refined cell parameters and the positional coordinates of PMN-0.36PT at different temperatures are given in Table IV.

Figure 16 shows the variation of the atomic displacements with temperature in the monoclinic and tetragonal phase regions. It is evident from this figure that in the monoclinic region, x_{Ti} and z_{O2} are close to zero within their estimated standard deviations. The z_{O1}, x_{O1}, and x_{O2} displacements are very small and do not change significantly with temperature. Largest contribution to polarization in the monoclinic (*Pm*) phase comes from z_{O3}, z_{Ti}, and x_{O3} displacements. In the monoclinic region, the x displacements are smaller for PMN-0.36PT than in PMN-0.32PT. All the atomic shifts change discontinuously across the *Pm*-*P*4*mm* phase boundary indicating first-order character of the phase transition. Coexistence of monoclinic and tetragonal phases over a wider range of temperatures also favors this conclusion. In the tetragonal region, the atomic displacements continuously decrease with increasing temperature, and discontinuously drop to zero at the *P*4*mm*-*Pm*3*m* phase boundary suggesting first order nature of this transition also.

IV. A NEW PHASE DIAGRAM OF PMN-*x*PT

Several workers have discussed the structure of PMN-*x*PT using single crystal specimens[4,27,28,31,50–52,54,55] and have proposed phase diagrams also.[4,31] However, the results of the single crystal studies should be treated with great caution since single crystals may possess large compositional gradients and segregation which are avoidable in ceramics. As a result, the local composition may differ very much from the nominal composition within the same single crystal.[49,54] As pointed out by Ye *et al.*,[54] a compositional fluctuation of ±5% is not uncommon in single crystals. As a result, phase diagrams of PMN-*x*PT, plotted on the basis of single crystal data, may not be reliable. For example, Shrout *et al.*[4] have reported rhombohedral symmetry in PMN-*x*PT single crystals for $x=0.30$, 0.35, and 0.40 (see Table I of Ref. 4) whereas the correct symmetry as determined using chemically homogeneous ceramic samples are found to be monoclinic M_B for $x=0.30$ and tetragonal for $x \geqslant 0.35$ with a coexisting M_C phase.[11] Similarly, the rhombohedral structure reported by Ye *et al.*[54] for PMN-0.35PT single crystals in unpoled state is incorrect. Further, the Curie point (T_C) of about 420 K reported by Tu *et al.*[27] for PMN-0.33PT rhombohedral crystal corresponds to the Curie point of PMN-0.29PT ceramics in the present work [see Fig. 1(c)]. The correct average composition of PMN-*x*PT crystals studied by Tu *et al.*[27] should therefore be $x=0.29$ and not $x=0.33$. Thus, while dealing with single crystals one may not be always sure about the actual composition, unless careful compositional analysis has been carried out, and any explanation of phase transition sequences based on nominal compositions may lead to erroneous conclusions. Therefore, for constructing the phase diagram, it is better to use chemically homogeneous ceramic samples, where the compositions are more reliable.

The temperature dependent dielectric constant, piezoelectric resonance frequency (Figs. 2 and 4) and structural studies using powder neutron diffraction data presented in the preceding sections have enabled us to construct a phase diagram of PMN-*x*PT system. Fig. 17 shows the new and updated phase diagram of PMN-*x*PT. The Curie points for the transition between the ferroelectric and the paraelectric phases were determined by dielectric measurements at 1 kHz on unpoled samples during heating whereas the second transition involving two ferroelectric phases (i.e., tetragonal and monoclinic phases) was determined using dielectric constant and/or piezoelectric resonance frequency measurements. The Curie points shown in Fig. 17 are slightly higher than those reported by Noblanc *et al.*[32] but are in agreement with those reported by Guo *et al.*[14] The values of Curie points shown in Fig. 17 are more reliable since they are consistent with the linear variation of T'_m as a function of composition from the $PbTiO_3$ end to the PMN end. It should be noted here that Noblanc *et al.*[32] have used 0.35 mol. % manganese oxide while synthesizing the samples to increase the breakdown strength. This might be the reason for lower transition temperatures in their samples. Our samples correspond to stoichiometric compositions free from any additives like manganese oxide and also the unwanted pyrochlore phase.

We now proceed to discuss the salient features of the modified phase diagram. The cubic paraelectric phase of PMN-*x*PT first transform into a relaxor state (R_E) for $x<0.35$. This relaxor phase undergoes Vogel-Fulcher freezing below the main Curie point. The continuous line passing through the open circles represents the variation of the Vogel-Fulcher freezing temperature with composition. Below this line, ferroelectric phases with different crystallographic

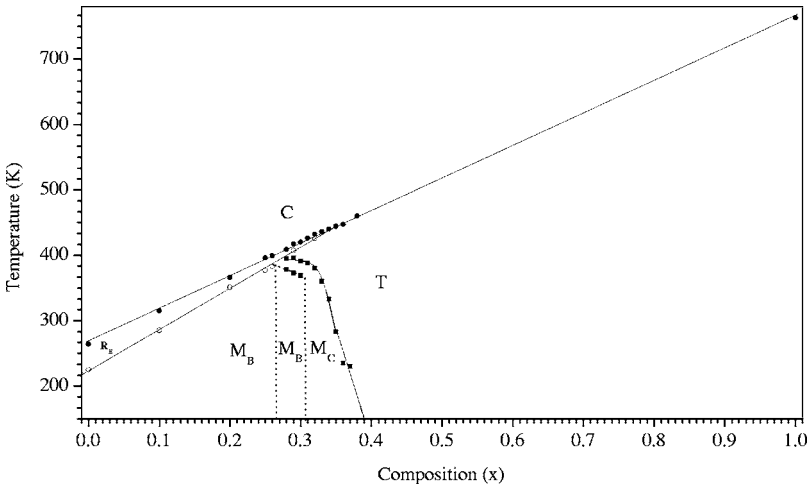

FIG. 17. Phase diagram of PMN-xPT showing the stability region of the pseudorhombohedral M_B, monoclinic M_B and M_C, tetragonal and cubic phases. The transition temperatures between ferroelectric and paraelectric cubic phase were determined by dielectric measurements on unpoled samples under heating whereas the second transition from tetragonal to monoclinic phase was determined using dielectric constant and/or piezoelectric resonance frequency measurements.

symmetries appear. For $x<0.27$, the ferroelectric phase shows pseudorhombohedral features but, as discussed in earlier sections, *its* symmetry is monoclinic of M_B type with *Cm* space group. For $0.27\leqslant x\leqslant 0.35$, the symmetry of the ferroelectric phase below the Vogel-Fulcher freezing temperature is tetragonal with *P*4*mm* space group. For $x>0.35$, there is no intermediate relaxor ferroelectric state, and the structure is tetragonal below the main Curie point. In the composition range $0.27\leqslant x\leqslant 0.30$, the tetragonal phase transforms successively into the monoclinic M_C (space group *Pm*) and M_B phases on lowering the temperature. For $0.30<x\leqslant 0.40$, the tetragonal phase transforms into the monoclinic M_C phase which remains stable down to the lowest temperature. Thus the ground state of PMN-xPT corresponds to the M_B phase for $x\leqslant 0.30$, M_C for $0.31\leqslant x\leqslant 0.40$ and tetragonal for $x>0.40$. It would be interesting to verify these ground states using first principles calculations.

The dotted vertical line shows an invariant point at $T\approx 392$ K corresponding to $x\approx 0.27$ where three stability fields corresponding to M_B, M_C, and tetragonal phases meet, if we ignore the metastable relaxor phase above T_{VF} line. The phase boundary between the monoclinic M_C and the tetragonal phases has been shown as a vertical line by Noheda *et al.*[24] at low temperatures. However, as can be seen from Fig. 17, this phase boundary is slanted even at low temperatures. The M_B-M_C phase boundary, on the other hand, is found to be extremely steep and sharp. The highest d_{33} value of PMN-xPT single crystals ($\sim$2500) at room temperature is found to correspond to the steep M_B-M_C phase boundary at $x\approx 0.30$.[31] It appears that the M_B-M_C phase boundary is the *real* MPB in the sense in which it was first introduced in the PZT ceramics.[2] The slanted M_C-tetragonal phase boundary leads to the second peak in the d_{33} versus x plot but with considerably lower value of d_{33} ($\sim$1500) at room temperature.[31]

V. CONCLUSIONS

Temperature dependent dielectric constant, piezoelectric resonance frequency and powder neutron diffraction studies on PMN-xPT compositions across MPB reveal several interesting phase transition sequences. These studies have enabled the construction of a new phase diagram for this system showing stability fields of ergodic relaxor, monoclinic M_B, monoclinic M_C, tetragonal and cubic phases. The M_B type monoclinic phase (space group *Cm*) for $0.27\leqslant x\leqslant 0.30$ transforms successively to the monoclinic M_C, tetragonal and cubic phases on heating above room temperature. The M_C type monoclinic phase (space group *Pm*) for $0.31\leqslant x\leqslant 0.34$ transforms successively to the tetragonal and cubic phases on heating above room temperature. The tetragonal phase with compositions close to the MPB transforms to the M_C type monoclinic phase on cooling below room temperature. Rietveld analyses of the powder neutron diffraction data below room temperature on a pseudorhombohedral composition with $x=0.25$ suggest that the short range M_B type monoclinic order present at room temperature can grow to long range monoclinic order on lowering the temperature. The compositions $x\geqslant 0.35$ with tetragonal structure at room temperature exhibit normal ferroelectric transition, whereas the nontetragonal compositions ($x<0.35$) exhibit relaxor ferroelectric type transition. All the structural transitions are found to be accompanied with anomalies either in the temperature dependence of dielectric constant or the piezoelectric resonance frequency or both.

ACKNOWLEDGMENTS

A.K.S. thanks CSIR for financial support. Neutron powder diffraction patterns were recorded at the SINQ, Paul Scherrer Institute, Villigen, Switzerland. The assistance of D. Cheptiakov is gratefully acknowledged.

*Email address: dapandey@bhu.ac.in

[1] K. Uchino and J. R. Giniewicz, *Micromechatronics* (Marcel Dekker Inc., New York, 2003).
[2] B. Jaffe, W. R. Cook, and H. Jaffe, *Piezoelectric Ceramics* (Academic Press, London/New York, 1971).
[3] S. W. Choi, T. R. Shrout, S. J. Jang, and A. S. Bhalla, Mater. Lett. **8**, 253 (1989).
[4] T. R. Shrout, Z. P. Chang, N. Kim, and S. Markgraf, Ferroelectr., Lett. Sect. **12**, 63 (1990).
[5] J. Kelly, M. Leonard, C. Tantigate, and A. Safari, J. Am. Ceram. Soc. **80**, 957 (1997).
[6] J. Kuwata, K. Uchino, and S. Nomura, Ferroelectrics **37**, 531 (1973).
[7] B. Noheda, D. E. Cox, G. Shirane, R. Guo, B. Jones, and L. E. Cross, Phys. Rev. B **63**, 014103 (2001).
[8] Ragini, R. Ranjan, S. K. Mishra, and D. Pandey, J. Appl. Phys. **92**, 3266 (2002).
[9] R. Ranjan, Ragini, S. K. Mishra, D. Pandey, and B. J. Kennedy, Phys. Rev. B **65**, 060102(R) (2002); D. M. Hatch, H. T. Stokes, R. Ranjan, Ragini, S. K. Mishra, D. Pandey, and B. J. Kennedy, *ibid.* **65**, 212101 (2002).
[10] A. K. Singh and D. Pandey, J. Phys.: Condens. Matter **13**, L931 (2001).
[11] A. K. Singh and D. Pandey, Phys. Rev. B **67**, 064102 (2003).
[12] J. M. Kiat, Y. Uesu, B. Dkhil, M. Matsuda, C. Malibert, and G. Calvarin, Phys. Rev. B **65**, 064106 (2002).
[13] B. Noheda, D. E. Cox, G. Shirane, S.-E. Park, L. E. Cross, and Z. Zhong, Phys. Rev. Lett. **86**, 3891 (2001).
[14] R. Guo, L. E. Cross, S. E. Park, B. Noheda, D. E. Cox, and G. Shirane, Phys. Rev. Lett. **84**, 5423 (2000).
[15] K.-P Chen, X.-W. Zhang, and H.-S. Luo, J. Phys.: Condens. Matter **14**, L571 (2002).
[16] X. Zhao, J. Wang, H. L. W. Chan, C. L. Choy, and H. Luo, J. Phys.: Condens. Matter **15**, 6899 (2003).
[17] B. Noheda, Z. Zhong, D. E. Cox, G. Shirane, S. E. Park, and P. Rehrig, Phys. Rev. B **65**, 224101 (2002).
[18] D.-S. Paik, S. Wada, S.-F. Liu, and T. Shrout, J. Appl. Phys. **85**, 1080 (1999).
[19] F. Bai, J. F. Li, and D. Viehland, Appl. Phys. Lett. **85**, 2313 (2004).
[20] A. A. Bokov and Z.-G. Ye, Appl. Phys. Lett. **95**, 6347 (2004); D. Viehland, J. F. Li, and E. V. Colla, J. Appl. Phys. **96**, 3379 (2004).
[21] L. Bellaiche and D. Vanderbilt, Phys. Rev. Lett. **83**, 1347 (1999); L. Bellaiche, A. Garcia, and D. Vanderbilt, *ibid.* **84**, 5427 (2000); L. Bellaiche, A. Garcia, and D. Vanderbilt, Phys. Rev. B **64**, 060103(R) (2001); H. Fu and R. E. Cohen, Nature (London) **403**, 281 (2000).
[22] D. Vanderbilt and M. H. Cohen, Phys. Rev. B **63**, 094108 (2001).
[23] D. Pandey, Ragini, Z. Kristallogr. **218**, 1 (2003).
[24] B. Noheda, D. E. Cox, G. Shirane, J. Gao, and Z.-G. Ye, Phys. Rev. B **66**, 054104 (2002).
[25] D. La-Orauttapong, B. Noheda, Z.-G. Ye, P. M. Gehring, J. Toulouse, D. E. Cox, and G. Shirane, Phys. Rev. B **65**, 144101 (2002).
[26] A. K. Singh, D. Pandey, and O. Zaharko, Phys. Rev. B **68**, 172103 (2003).
[27] C. S. Tu, V. H. Schmidt, I.-C. Shih, and R. Chien, Phys. Rev. B **67**, 020102(R) (2003).
[28] C. S. Tu, I.-C. Shih, V. H. Schmidt, and R. Chien, Appl. Phys. Lett. **83**, 1833 (2003).
[29] D. Viehland and J. F. Li, J. Appl. Phys. **92**, 7690 (2002).
[30] V. Y. Topolov and Z.-G. Ye, Phys. Rev. B **70**, 094113 (2004).
[31] Y. Guo, H. Luo, D. Ling, H. Xu, T. He, and Z. Yin, J. Phys.: Condens. Matter **15**, L77 (2003).
[32] O. Noblanc, P. Gaucher, and G. Calvarin, J. Appl. Phys. **79**, 4291 (1996).
[33] E. V. Colla, E. L. Furman, S. M. Gupta, N. K. Yushin, and D. Viehland, J. Appl. Phys. **83**, 3298 (1998).
[34] J. Han and W. Cao, Phys. Rev. B **68**, 134102 (2003).
[35] G. Shirane, R. Pepinsky, and B. C. Frazer, Acta Crystallogr. **9**, 131 (1956).
[36] A. K. Singh and D. Pandey (to be published).
[37] S. L. Swartz and T. R. Shrout, Mater. Res. Bull. **17**, 1245 (1982), O. Bouquin, L. Martine, J. Am. Ceram. Soc. **74**, 1152 (1991); H. C. Wang and W. A. Schulze, *ibid.* **73**, 825 (1990).
[38] R. A. Young, A. Sakthivel, T. S. Moss, and C. O. Paiva Santos, Program DBWS-9411 for Rietveld Analysis of x-ray and Neutron Powder Diffraction Pattern (1994); J. Rodriguez-Carvajal, Fullprof, Laboratoire Leon Brillouin (CEA-CNRS), France (2001).
[39] D. Pandey, Key Eng. Mater. **101-102**, 177 (1995).
[40] L. E. Cross, Ferroelectrics **76**, 241 (1987).
[41] D. Viehland, J. F. Li, S. J. Jang, L. E. Cross, and M. Wuttig, Phys. Rev. B **43**, 8316 (1991).
[42] D. Viehland, S. J. Jang, L. E. Cross, and M. Wuttig, J. Appl. Phys. **68**, 2916 (1990); O. Bidault, M. Licheron, E. Husson, G. Calvarin, and A. Morell, Solid State Commun. **98**, 765 (1996).
[43] Ragini, S. K. Mishra, D. Pandey, H. Lemmens, and G. Van Tendeloo, Phys. Rev. B **64**, 054101 (2001).
[44] D. L. Corker, A. M. Glazer, R. W. Whatmore, A. Stallard, and F. Fauth, J. Phys.: Condens. Matter **10**, 6251 (1998).
[45] P. W. Stephens, J. Appl. Crystallogr. **32**, 281 (1999).
[46] A. M. Glazer, P. A. Thomas, K. Z. Baba-Kishi, G. K. H. Pang, and C. W. Tai, Phys. Rev. B **70**, 184123 (2004).
[47] S. Wakimoto, C. Stock, R.J. Birgeneau, Z.-G. Ye, W. Chen, W. J. L. Buyers, P. M. Gehring, and G. Shirane, Phys. Rev. B **65**, 172105 (2002).
[48] G. Xu, D. Viehland, J. F. Li, P. M. Gehring, and G. Shirane, Phys. Rev. B **68**, 212410 (2003).
[49] D. Zekria and A. M. Glazer, J. Appl. Crystallogr. **37**, 143 (2004).
[50] Y. Guo, H. Luo, K. Chen, H. Xu, X. Zhang, and Z. Yin, J. Appl. Phys. **92**, 6134 (2002).
[51] Z. Feng, X. Zhao, and H. Luo, J. Phys.: Condens. Matter **16**, 3769 (2004); Solid State Commun. **130**, 591 (2004).
[52] Yu Lu, D.-Y, Z.-Y. Cheng, Q. M. Zhang, H.-S. Luo, Z.-W. Yin, and D. Viehland, Appl. Phys. Lett. **78**, 3109 (2001).
[53] I. A. Sergienko, Y. M. Gufan, and S. Urazhdin, Phys. Rev. B **65**, 144104 (2002).
[54] Z. G. Ye and M. Dong, J. Appl. Phys. **87**, 2312 (2000).
[55] Z. G. Ye, B. Noheda, M. Dong, D. Cox, and G. Shirane, Phys. Rev. B **64**, 184114 (2001).